Applied Energy 421 (2026) 128210

Contents lists available at ScienceDirect

Applied Energy

journal homepage: www.elsevier.com/locate/apenergy

# Spatiotemporal supply-demand matching in residential building rooftop photovoltaics (PV) under climate change: a cross-climate zone assessment

Zhuocheng Duan [a,*], Shady Attia [b], Hossein Omrany [a], Ruidong Chang [a], Jian Zuo [a]

[a] School of Civil Engineering and Construction Management, Adelaide University, Australia
[b] Sustainable Building Design Lab, Dept. UEE, Faculty of Applied Sciences, University of Liège, Belgium

## HIGHLIGHTS

- Multi-scale analysis across 27 cities in ASHRAE zones quantifies climate-driven PV-demand mismatches under climate change.
- Zone 0 faces compound risks: demand rises 33.6–38.5%, SSR declines from 48.2 to 50.9% (baseline) to 46.5–49.0% (SSP585_2080).
- Cool to cold regions in Zones 5–6 achieve 11.3–19.5% energy reductions but winter SSR typical remains below 15% due to astronomical constraints.
- Extremes drive up to 4× energy deficits in tropics heat events and 37–57 zero-generation days in polar zones.
- Climate-driven patterns persist across building envelope variations and PV capacity changes (50–150% baseline).

## GRAPHICAL ABSTRACT

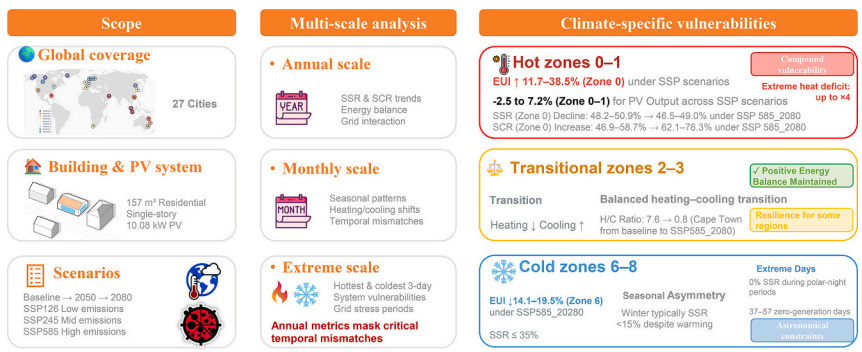


## ARTICLE INFO

*Keywords:*
Self-sufficiency
Self-consumption
Heating and cooling demand
Solar renewable energy
Zero energy buildings
Carbon emissions

## ABSTRACT

The building sector accounts for over one-third of global energy use and emissions, making on-site renewable generation critical for climate neutrality. Rooftop photovoltaics (PV) can reduce reliance on fossil fuels, yet climate change alters both building energy demand and PV output, creating poorly understood spatiotemporal mismatches. To bridge this gap, this study employed a multi-scale temporal analysis across 27 cities representing all ASHRAE climate zones, integrating extreme event assessment with traditional annual metrics to reveal unique PV-demand matching dynamics. A single-storey residential building with 10.08 kW rooftop PV was simulated via Ladybug tools (EnergyPlus engine) in Rhino under baseline, SSP126, SSP245 and SSP585 scenarios (2050, 2080) to analyze self-sufficiency ratio (SSR) and self-consumption ratio (SCR) at annual, monthly and daily scales.

*Abbreviations:* SDGs, Sustainable Development Goals; GHG, Greenhouse Gas; UN, United Nations; HVAC, Heating, Ventilation, and Air Conditioning; SSP, Shared Socioeconomic Pathways; CMIP6, Coupled Model Intercomparison Project Phase 6; PV, Photovoltaic; IRENA, International Renewable Energy Agency; RCP, Representative Concentration Pathway; SCR, Self-Consumption Ratio; SSR, Self-Sufficiency Ratio; ASHRAE, American Society of Heating, Refrigerating and Air-Conditioning Engineers; ACH, Air Changes per Hour; UAE, United Arab Emirates; EUI, Energy Use Intensity; VRF, Variable Refrigerant Flow; DC, Direct Current; AC, Alternating Current; WWR, Window-to-Wall Ratio; IECC, International Energy Conservation Code; GHI, Global Horizontal Irradiation; IEA, International Energy Agency; COP, Coefficient of Performance; EPW, EnergyPlus Weather; GCM, General Circulation Model; NZEB, Nearly Zero Energy Building; SHGC, Solar Heat Gain Coefficient.

* Corresponding author.
*E-mail address:* zhuocheng.duan@adelaide.edu.au (Z. Duan).

https://doi.org/10.1016/j.apenergy.2026.128210
Received 22 August 2025; Received in revised form 31 May 2026; Accepted 6 June 2026
Available online 20 June 2026
0306-2619/© 2026 The Author(s). Published by Elsevier Ltd. This is an open access article under the CC BY license (http://creativecommons.org/licenses/by/4.0/).

Under SSP585_2080, extreme hot regions (Zone 0) face compound vulnerabilities: energy demand rises 33.6–38.5% while PV output changes marginally (−2.5% to 4.0%), reducing SSR from 48.2–50.9% (baseline) to 46.5–49.0%, despite SCR increases to 62.1–76.3%. Cool and cold regions in Zones 5–6 benefit from 11.3–19.5% demand reductions (SSP585_2080) but remain limited by winter generation, with SSR constrained at 24.0–35.6% under the same scenario. Monthly analysis exposes seasonal asymmetries with high-latitude (Zones 6–8) winter SSR typically below 15% despite warming. Most critically, extreme-event analysis exposed up to fourfold increases in energy deficits during extreme heat events in tropical zones and confirmed the expected zero PV generation during polar nights, a fundamental limitation that persists despite warming and that annual metrics consistently obscure. Sensitivity analysis examining building envelope performance variations and PV system capacity changes confirmed climate-driven performance patterns. These findings demonstrate heterogeneous climate change impacts that fundamentally challenge universal renewable energy targets, necessitating coordinated strategies combining demand-side interventions, climate-specific renovation and supplementary energy sources to address inherent solar limitations. Such insights provide essential guidance for renewable energy policy development and urban energy planning.

## 1. Introduction

### 1.1. Climate change and the building sector

Global warming is widely regarded as one of the most significant challenges facing the planet. This critical situation has driven global responses and initiatives such as the Paris Agreement and the Sustainable Development Goals (SDGs) [1,2], to reduce greenhouse gas (GHG) emissions and promote sustainable energy practices. Specifically, to align with the SDG 7 (affordable and clean energy), SDG 11 (sustainable cities and communities) and SDG 13 (climate action), urgent innovative solutions are needed in both the energy sector and the built environment.

The building and construction sector stands at the critical nexus of climate change mitigation and adaptation efforts. According to UN reports on global building status of 2023 [3], the building sector accounted for approximately 34% of global energy consumption as well as associated emissions. Despite these advancements and efforts, the sector is not on track to achieve net-zero carbon by 2050 [4]. Significantly, emissions have increased by 5% since 2015, falling far short of the 28% reduction required by the Paris Agreement [3]. Such a high proportion makes buildings a primary target for decarbonization strategies and clean energy integration.

The building sector and global warming are characterized by a self-reinforcing loop [5]. On the one hand, rising temperature patterns, increased frequency of extreme weather events, and altered solar radiation regimes directly influence building thermal performance [6,7]. On the other hand, emissions from HVAC energy consumption and building materials further contribute to climate forcing. These dual challenges: reducing emissions while adapting to climate change, necessitate transformative approaches and effective energy conservation measures for building energy systems [8,9].

### 1.2. Future building thermal performance

The building scientific community has made substantial progress in developing methodologies to assess future building energy performance through simulation. For instance, Belcher et al. [10] proposed the most widely utilized morphing method to downscale the climate models for future weather files, which became foundational for subsequent research. Jentsch et al. [11] expanded on this work by creating the CCWorldWeatherGen tool to generate three time slices (2020s, 2050s and 2080s) under the A2 scenario. However, the earlier climate model became increasingly outdated as climate science has advanced. Addressing this limitation, Rodrigues et al. [12] proposed an open-source morphing tool under more current Shared Socioeconomic Pathways (SSP) scenarios. Shen [13] employed distribution adjusted temporal mapping techniques to generate future SSP weather files using the MRI-ESM2–0 model, validating results with observed data from 2015 to 2024 and thereby enhancing the reliability of future projections.

These methodological advances have enabled researchers to quantify how climate change significantly alters building thermal performance through shifts in heating and cooling demands driven by rising temperatures, more frequent and intense extreme weather events, as well as changing humidity levels [14]. Most notably, these impacts create divergent effects across different building thermal performance profiles and climate zones [15–17]. In warmer climates, cooling demand is projected to surge, while heating demand will decline significantly in colder regions, resulting in spatially varied energy consumption patterns [15]. Zou et al. [17] reported decreases in energy use in cold regions, small reductions in temperate zones due to offsetting cooling increases and heating decreases, and substantial increases in regions where cooling demands dominate the energy consumption. Such regionally diverse outcomes underscore the complexity of climate adaptation strategies and highlight the need for context-specific approaches to building energy management [8,9].

Beyond energy consumption patterns, building performance under climate change encompasses critical dimensions of thermal comfort and environmental impact. Rahif et al. [18] revealed 154–528% increases in overheating risk coupled with up to 32% reduction in overcooling risk by the 2090s, demonstrating profound implications for occupant well-being and productivity. Akkose et al. [19] investigated the future thermal performance of educational buildings under global warming with urban heat island effects, and reported that indoor overheating degrees almost doubled in 2060 in June.

### 1.3. Photovoltaic (PV) integration and climate change complexity

As global energy demands continue to rise and the imperative to decarbonize intensifies to mitigate the far-reaching consequences of climate change, renewable energy integration, particularly through photovoltaic (PV) systems, offers a compelling solution for on-site renewable energy generation and the transformation of building energy systems. According to the International Renewable Energy Agency (IRENA) [20], global PV capacity has experienced unprecedented growth, increasing from 100 GW in 2012 to 1411 GW in 2023 (a fourteen-fold increase), with costs declining dramatically (up to 93% between 2010 and 2020). This remarkable growth trajectory has positioned solar PV as a cornerstone of sustainable building strategies worldwide.

Incorporating solar technologies into building designs delivers multiple benefits: it improves energy efficiency, reduces carbon emissions, and alleviates grid burden, particularly critical given the accelerating electrification of HVAC systems and transport [21,22]. Rooftop PV systems have emerged as a particularly viable solution due to their retrofit compatibility, established deployment practices and substantial generation potential. However, climate change introduces significant complexity to PV system performance by simultaneously affecting both building energy demands and PV generation capacity. Rising temperatures shift heating and cooling loads, alter peak demand patterns and

impact PV efficiency [23]. Moreover, changes in solar radiation and extreme weather events directly impact PV generation capacity and reliability [24]. Global assessments of renewable (wind and solar) energy systems reveal that climate change fundamentally disrupts supply-demand matching [25]. At the building scale, Tamer et al. [26] investigated future heating, cooling and PV generation across 81 Turkish cities, with specific focus on associated carbon footprint and energy cost, though their focus remained on annual metrics rather than temporal matching dynamics. Research on nearly zero energy buildings (NZEBs) indicates that high-performance building systems are better able to cover their building loads under global warming scenarios [27]. This improved performance stems from superior envelope design that minimizes heating and cooling demands, creating more favorable supply-demand matching conditions even as climate conditions shift.

The literature reveals substantial geographic variation in projected climate impacts on PV performance. This spatial heterogeneity results from several factors including (1) alterations in solar radiation patterns, cloud cover driven by atmospheric circulation changes, and (2) different climate models (GCMs and RCMs) and downscaling methods. For instance, D'Agostino [27] reported increased PV output in European case studies under Representative Concentration Pathway (RCP) 8.5 in 2060, with a 6% increase in Milan and more than 20% increase in Vienna due to lower cloud cover. De Masi et al. [24] reported increases for all future monthly PV output with varying magnitudes across different scenarios (RCP4.5 and RCP8.5) in Italy. However, Ahmadian et al. [28] confirmed a 0.6% decrease in 2050 PV generation in London compared to the baseline. These regional differences are further substantiated by Guo et al. [29], who investigated future PV generation trends in China using Coupled Model Intercomparison Project Phase 6 (CMIP6) models. They reported that annual output will decrease by up to 4% in Tibet and northern China under SSP585, while the largest increases exceed 10% in southern and central China under SSP126. While PV represents one component of comprehensive renewable energy strategies, understanding the temporal dynamics between PV generation and building energy consumption is important for optimizing on-site renewable integration and informing decisions about complementary technologies such as energy storage, demand management and grid flexibility measures.

### 1.4. Research gaps and study objectives

Despite extensive research on individual aspects of the impact of climate change on building thermal performance, critical knowledge gaps persist that fundamentally limit our ability to design climate-resilient PV-building energy systems under global warming.

Table S1 in supplementary material (SM) synthesizes relevant prior studies on multi-climate PV/building research. First, there exists a spatial-methodological gap in systematic cross-climate comparative analysis of coupled building-PV systems under future scenarios. While previous studies examine either building performance [15–17] or PV generation [26,29,30] independently, single-location studies have advanced understanding of load-matching dynamics. Nevertheless, none has systematically quantified the dynamic interactions between building energy consumption and PV generation across all ASHRAE climate zones under a consistent methodological framework spanning both current and future climates. This integration is critical because climate change simultaneously affects both generation capacity and energy demand patterns. The resulting feedback loops vary substantially across geographic regions yet remain poorly characterized at the cross-climate scale. Existing studies are predominantly single-location and climate-static. Existing research therefore lacks the systematic comparative framework necessary to identify climate-specific vulnerabilities and transferable design principles.

Second, there persists a critical temporal-resilience gap in building-PV performance assessment under climate change. While Luthander et al. [31] established self-consumption ratio (SCR) and self-sufficiency ratio (SSR) as fundamental temporal-matching metrics, subsequent work refined these metrics for individual climates and explored the roles of battery storage and electric vehicles [32–35]. However, annual energy balance metrics dominate the literature [26]. Such metrics cannot capture the temporal mismatches that determine real-world system viability and grid stability. Systematic analysis spanning multiple temporal scales (annual, monthly and daily) across ASHRAE climate zones and multiple SSP scenarios remains absent. Furthermore, climate change intensifies extreme weather events, raising significant concerns about grid stress, resilience failures, and compound supply-demand vulnerabilities in renewable energy systems [22,36]. Yet no framework evaluates PV contribution to building resilience during such events across climatically diverse locations. This gap is particularly consequential because system resilience is determined by performance during supply-demand mismatches and extreme events rather than annual averages. The magnitude and patterns of these compound vulnerabilities remain unquantified across climate zones.

The present study makes three verifiable contributions relative to prior literature (Table S1):

1. Cross-climate comprehensiveness. This study provides systematic assessment of building energy consumption and rooftop PV generation across ASHRAE climate zones, covering 27 globally distributed cities under a single consistent simulation framework.
2. Multi-scale temporal matching under multi-scenario future climates. Supply-demand matching is quantified at annual, monthly and daily scales under a multi-model CMIP6 ensemble spanning SSP126, SSP245, and SSP585 in 2050 and 2080.
3. Extreme-event resilience assessment. A framework evaluates PV contribution to building self-sufficiency during heat and cold spell events, quantifying compound supply-demand vulnerabilities that annual metrics alone cannot capture.

To address these gaps, this study quantifies building rooftop PV supply-demand matching across all ASHRAE climate zones under multiple future scenarios and temporal scales. This multi-zone comparative approach provides valuable insights for researchers, building designers, energy policymakers and PV system engineers. Specifically, this research aims to explore: 1) How will climate change influence building-PV performance across ASHRAE climate zones under multiple climate scenarios? 2) How does temporal matching between PV generation and building energy consumption evolve across multiple time scales (annual, monthly and daily extreme patterns) under different climate scenarios? By doing so, it aims to develop recommendations for climate-responsive building energy systems that maximize renewable energy utilization and enhance resilience to a warming climate. The findings will contribute to improving building energy efficiency, enhancing renewable energy integration, and ultimately supporting global efforts toward climate resilience and carbon neutrality.

## 2. Materials and methods

### 2.1. Climate zone classification

The ASHRAE climate zone classification system provides a standardized framework for categorizing global climate conditions relevant to building thermal performance, which has already been adopted in previous building energy research [16,37]. This building-centric approach directly captures variables affecting both energy consumption and PV generation, essential for understanding PV-building energy dynamics. This system categorizes regions based on temperature and moisture regimes, ranging from extremely hot to subarctic [38], and each major zone can be further subdivided based on moisture conditions: moist (A), dry (B), and marine (C). The representative cities in Table 1 were selected for this study, and their classification was obtained based on the *Climatic Data for Building Design Standards* [39]. This

**Table 1**
Selected cities in different ASHRAE climate zones.

| ASHRAE Climate Zone | City | Country/ Region | Latitude | Longitude |
|---|---|---|---|---|
| Zone 0 | Singapore | Singapore | 1.36 | 103.91 |
| | Dubai | UAE | 25.25 | 55.36 |
| | Jakarta | Indonesia | −6.16 | 106.84 |
| Zone 1 | Townsville | Australia | −19.25 | 146.77 |
| | Miami | US | 25.91 | −80.28 |
| | Shenzhen | China | 22.54 | 114 |
| Zone 2 | Guangzhou | China | 23.21 | 113.48 |
| | Brisbane | Australia | −27.38 | 153.13 |
| | Las Vegas | US | 36.21 | −115.2 |
| Zone 3 | Cape Town | South Africa | −33.92 | 18.44 |
| | Sydney | Australia | −33.93 | 151.17 |
| | Barcelona | Spain | 41.42 | 2.13 |
| Zone 4 | Seoul | South Korea | 37.53 | 126.97 |
| | London | UK | 51.51 | 0.06 |
| | Canberra | Australia | −35.3 | 149.2 |
| Zone 5 | Toronto | Canada | 43.67 | −79.4 |
| | Aarhus | Denmark | 56.08 | 10.14 |
| | Zurich | Switzerland | 47.38 | 8.57 |
| Zone 6 | Helsinki | Finland | 60.18 | 24.94 |
| | Oslo | Norway | 59.94 | 10.72 |
| | Stockholm | Sweden | 59.35 | 18.07 |
| Zone 7 | Harbin | China | 45.93 | 126.58 |
| | Edmonton | Canada | 53.57 | −113.52 |
| | Anchorage | US | 61.22 | −149.85 |
| Zone 8 | Fairbanks | US | 64.82 | −147.87 |
| | Sisimiut | Greenland | 66.95 | −53.72 |
| | Yellowknife | Canada | 62.46 | −114.44 |

classification framework enables systematic comparison of building energy performance and renewable energy generation across the full range of global climate conditions. However, we acknowledge an important limitation: current climate zone classification systems, including ASHRAE (based on temperature and moisture) and Köppen-Geiger (based on patterns of seasonal precipitation and temperature), do not incorporate solar radiation metrics as classification parameters.

### 2.2. Building energy modeling

A single-family residential building was strategically selected to ensure methodological consistency across climate zones while capturing the fundamental dynamics of building-PV interactions that are transferable across building typologies. This approach follows established precedent in cross-climate building energy research [27,40,41] where representative archetypes enable systematic isolation of climate-driven effects from building-specific variables. To ensure methodological consistency while acknowledging the limitations of a single archetype approach, all building simulations employed standardized operational parameters derived from ASHRAE standards in Ladybug tools, with comprehensive details provided in SM Table S2. The 157 $m^2$ single-storey residence with 40% window-to-wall ratio represents a simplified reference building that facilitates systematic comparison across diverse climates. The PV system was modeled using the Honeybee Photovoltaic Properties component and configured as a fixed roof-mounted array with an area of 70 $m^2$ and a DC capacity of 10.08 kW, with 16% rated efficiency (Table 2). To maintain methodological consistency and comparability, the simulations accounted for hemispheric differences in PV orientation. For Northern Hemisphere locations, panels were oriented southward (180° azimuth) to maximize solar exposure, while Southern Hemisphere locations (such as Australian cities) featured northward-facing panels (0° azimuth).

All building simulations were conducted using Ladybug tools (with the EnergyPlus engine) implemented within Grasshopper in Rhino. Occupant density was set at 0.028 persons/$m^2$, with internal heat gains of 6.67 W/$m^2$ for equipment and 9.36 W/$m^2$ for lighting, representing residential usage patterns. Occupancy schedules were kept consistent across all climate zones to isolate climate-driven effects from behavioral variations (Table S2). Variable refrigerant flow (VRF) systems were specified for heating and cooling, with coefficient of performance (COP) values calculated dynamically by EnergyPlus. Heat pump water heaters were modeled with a COP of 3.5 at standard rating conditions. HVAC setpoints were standardized at 21.7°C for heating and 24.4 °C for cooling across all locations. Infiltration rates were set at 0.000569 $m^3$/s per $m^2$ of facade area, and mechanical ventilation was set to 0.35 ACH.

**Table 2**
Detailed Building and PV system modeling.

| Parameter Category | Specification | Value/Description |
|---|---|---|
| Building Characteristics | Surroundings | 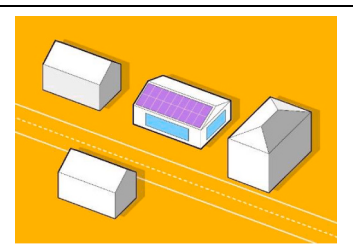 |
| | Floor Area ($m^2$) | 157.57 |
| | Roof Type | Pitched (22.2° slope) |
| | Building Envelope | ASHRAE 90.1-2019 / IECC 2021 standard |
| | Window-to-Wall Ratio | 40% |
| | HVAC System | Variable Refrigerant Flow (VRF) |
| | Hot Water System | Heat Pump Water Heater |
| PV system | Area ($m^2$) | 70 |
| | Mounting Type | Fixed Roof-Mounted |
| | Tilt Angle | 22.2° (aligned with roof pitch) |
| | DC Rated Capacity | 10.08 kW |
| | Rated Efficiency | 16% |
| | Active Fraction | 0.90 (Default) |
| | Loss Fraction | 0.14 (Default) |
| | Orientation (Northern Hemisphere) | South (180° azimuth) |
| | Orientation (Southern Hemisphere) | North (0° azimuth) |
| | DC-to-AC size | 1.25 |
| | Inverter Efficiency | 0.96 (Default) |

To ensure cross-climate comparability, the thermal properties of the building envelope were set according to ASHRAE climate zone specifications (ASHRAE 90.1-2019 / IECC 2021 standard) using the HB construction set by climate component in Ladybug 1.9 (Table S3).

This study employed several performance metrics to evaluate building-PV system integration. Building thermal performance was quantified through site energy use intensity (EUI, kWh/m$^2$/year), with breakdown by end-use categories (heating, cooling, lighting, etc.). For analyzing the temporal matching between generation and consumption, we evaluated the system using load matching indices including the SCR (percentage of PV generation directly consumed on-site) and the SSR (proportion of building energy met by on-site generation) [31]. Grid interaction in this study employs a simplified instantaneous energy balance approach without explicit modeling of tariff structures, net-metering policies, or curtailment mechanisms. At each hourly time-step, instantaneous energy flows are calculated as follows: (1) PV energy consumed on-site represents the minimum of PV generation and building consumption for that hour; (2) Grid import quantifies building consumption minus on-site PV consumption when demand exceeds generation; (3) Grid export represents PV generation minus on-site consumption when generation exceeds demand. This simplified framework enables systematic cross-climate comparison of temporal supply-demand matching patterns, however actual grid behavior involves additional complexity not captured in this analysis. These indices were calculated at multiple temporal resolutions (Eqs. (1) and (2)): annual values provided overall system performance benchmarks, while monthly analyses revealed seasonal relationships and daily analyses examined the resilience. For each city, scenario and period, the extreme hot and extreme cold 3-day events were identified independently from the corresponding 8760-h EPW file. A 72-h moving window was advanced across the full calendar year, and the mean outdoor dry-bulb air temperature was computed for each window. The hottest event was the window with the highest 3-day mean dry-bulb temperature; the coldest was the window with the lowest. No seasonal restriction was applied, and each selected event represents the most thermally stressful sustained period present in that scenario rather than a fixed calendar date. Where multiple windows shared an identical 3-day mean to the available numerical precision, the earliest occurrence was selected. As noted in Section 3.3, the selected dates differ across scenarios. The resulting differences therefore reflect combined changes in temperature extremes and concurrent solar conditions rather than an isolated climate-change signal on a fixed date.

Eq. (1): Self-Consumption Ratio (SCR)

$$SCR = \frac{E_{PV,cons}}{E_{PV,total}} \times 100\% \tag{1}$$

Eq. (2): Self-Sufficiency Ratio (SSR)

$$SSR = \frac{E_{PV,cons}}{E_{Load}} \times 100\% \tag{2}$$

Where:

$E_{PV,cons}$= *PV energy consumed directly by the building (kWh).*

$E_{PV,total}$= *total PV electricity generation (kWh).*

$E_{Load}$= *total building electricity demand (kWh).*

### 2.3. Future weather conditions

To generate future weather files, the study employed the open-source *Future Weather Generator* tool developed by Rodrigues et al. [12], which has been employed in previous studies [42–45]. The tool incorporates a 23-model CMIP6 ensemble comprising BCC-CSM2-MR, CanESM5, CanESM5.1, CanESM5-CanOE, CAS-ESM2.0, CMCC-ESM2, CNRM-CM6.1, CNRM-CM6.1-HR, CNRM-ESM2.1, EC-Earth3, EC-Earth3-Veg, EC-Earth3-Veg-LR, FGOALS-g3, GFDL-ESM4, GISS-E2.1-G, GISS-E2.1-H, GISS-E2.2-G, IPSL-CM6A-LR, MIROC-ES2H, MIROC-ES2L, MIROC6, MRI-ESM2.0, and UKESM1.0-LL, all contributing to the 6th IPCC Assessment Report [12]. These models were selected by the tool developers on the basis of complete data availability across all target SSP scenarios and morphing variables. For each month and city, the tool computes ensemble-mean monthly change deltas across all GCMs, applies bilinear interpolation to the city's precise coordinates, and morphs the baseline EPW parameters via shift, stretch, and a combination of both [10]. This procedure yields a single ensemble-mean morphed EPW file per city–scenario–period combination, which was subsequently used as the climate boundary condition for all simulations. The multi-model ensemble approach helps reduce uncertainty associated with individual model biases [46]. For future scenarios, the study utilized SSP126 (low emissions), SSP245 (intermediate emissions), and SSP585 (very high emissions) scenarios [18,47,48]. The SSP126 scenario represents a future with aggressive climate mitigation achieving net-zero $CO_2$ emissions, the SSP245 scenario represents a middle-of-the-road future with moderate mitigation efforts, while the SSP585 scenario describes a high-end emissions pathway that allows examination of the most severe warming potential [49]. These scenarios represent exogenous climate narratives rather than endogenous policy levers, providing boundary conditions for our analysis. To assess temporal evolution, three distinct periods were analyzed: baseline period (current climate conditions), mid-century period (2050) and late-century period (2080).

## 3. Results and discussion

### 3.1. Geographical distribution of temperature and solar radiation changes

Fig. 1 shows the average dry-bulb temperature increase across the studied cities and scenarios. By 2080, the SSP585 scenarios exhibit more pronounced warming (2–8 °C) compared to the SSP245 scenarios (1–5 °C) and SSP126 scenarios (1–3 °C). The most severe warming is witnessed in high-latitude regions (Fig. 1a), such as Yellowknife (7.1 °C), Helsinki (5.4 °C) and Fairbanks (6.6 °C) under SSP585_2080. Cities in the ASHRAE zones 6–8 experience more than 4 °C temperature increases in SSP585_2080. These findings highlight the warming potential in arctic and subarctic regions and their vulnerability. This pattern aligns with the established phenomenon of polar amplification. High-latitude regions in the northern hemisphere warm disproportionately due to positive local lapse-rate feedback and surface albedo feedback mechanisms [50].

Regarding average monthly temperature increases (Fig. 1b), cold regions (Zones 6–8) exhibit pronounced seasonal asymmetry in warming patterns, with winter months experiencing temperature increases 1.5–2 times greater than summer months. For cities in the subarctic Zone 8, temperature increases from December to February reach 9.0–9.7 °C compared to summer increases of 4.8–5.0 °C (June to August). In contrast, tropical and subtropical Zones (0–2) display more uniform warming (3–4 °C) throughout the year, with monthly temperature increases varying by less than 0.5 °C across seasons. The seasonal consistency in warming may lead to more straightforward adaptation challenges in hot climates (focused on addressing increased cooling loads) compared to more uncertain and complex situations in regions experiencing shifting weather patterns.

Solar radiation changes by city and scenario (Fig. 2) reveal distinct regional patterns that do not directly correspond to temperature increases. European cities, such as London, Zurich, Aarhus and Barcelona, consistently show substantial Global Horizontal Irradiation (GHI) increases across all scenarios (2.5–6.1%), potentially enhancing PV outputs in these regions. Conversely, extremely cold climate zones (7–8) exhibit consistent GHI decreases, with Anchorage (−6.4%), Sisimiut (−9.2%) and Fairbanks (−5.5%) showing the most substantial reductions under SSP585_2080, likely resulting from changes in cloud cover, precipitation patterns, and atmospheric moisture content. Tropical regions demonstrate considerable variability in solar radiation responses. Dubai shows a mixed response, with changes ranging from a slight decrease to a marginal increase (−1.8% to +1.1%), whereas

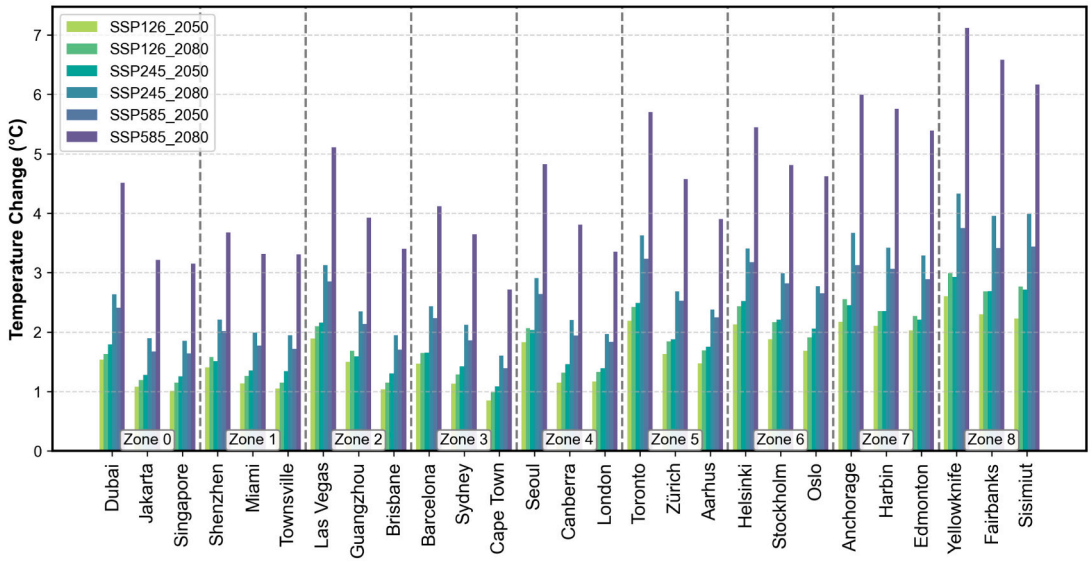


*a. Average annual temperature increases under SSP scenarios for 2050 and 2080*

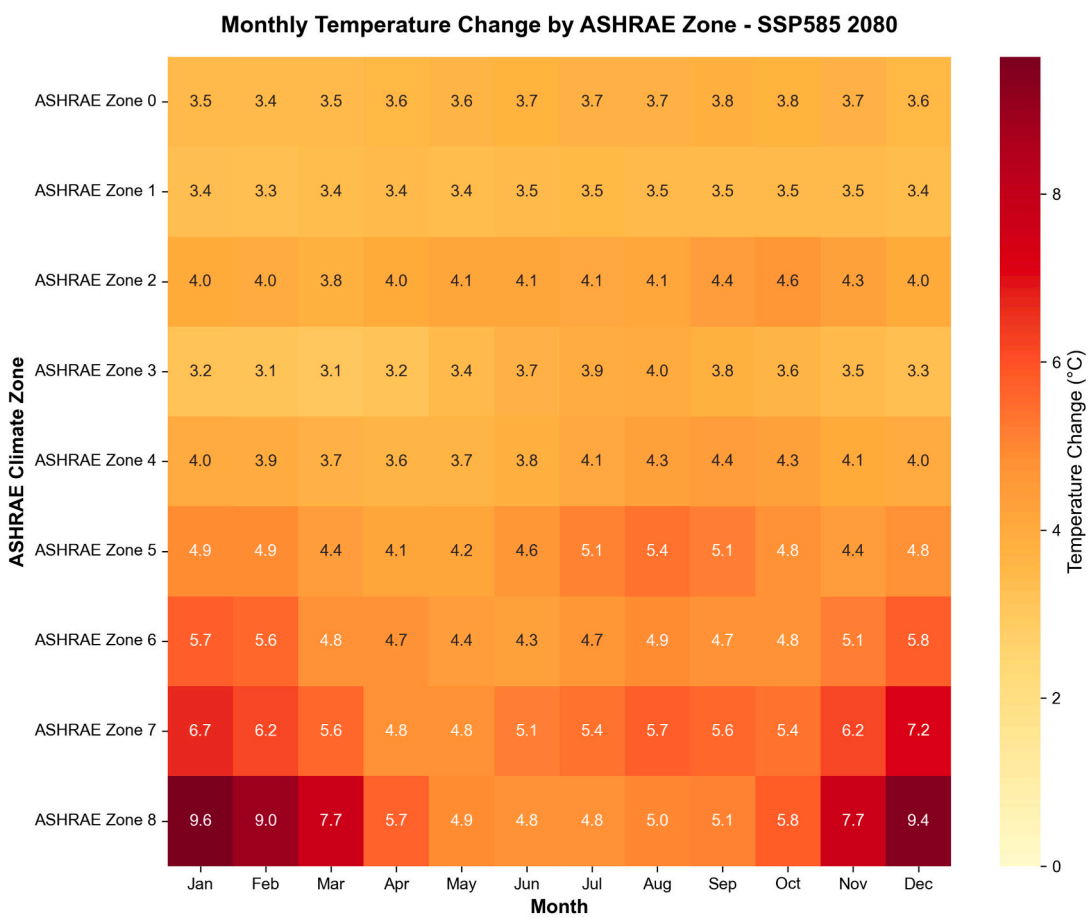


*b. Monthly changes under SSP585_2080.*

**Fig. 1.** Projected temperature changes by city and scenarios.

Guangzhou (2.7–8.8% increase) and Shenzhen (2.3–7.2% increase) consistently exhibit increasing trends, with the largest gains occurring under the SSP126_2080 scenario. Furthermore, the coldest cities (ASHRAE zones 7–8) display both the most substantial temperature increases and the most pronounced GHI decreases, particularly under the SSP585_2080 scenario. This reduces solar resource availability precisely where warming is most dramatic.

### 3.2. Baseline performance analysis

Baseline analysis provides the first level of understanding by establishing overall energy balance trends (Fig. 3). EUI exhibits a clear

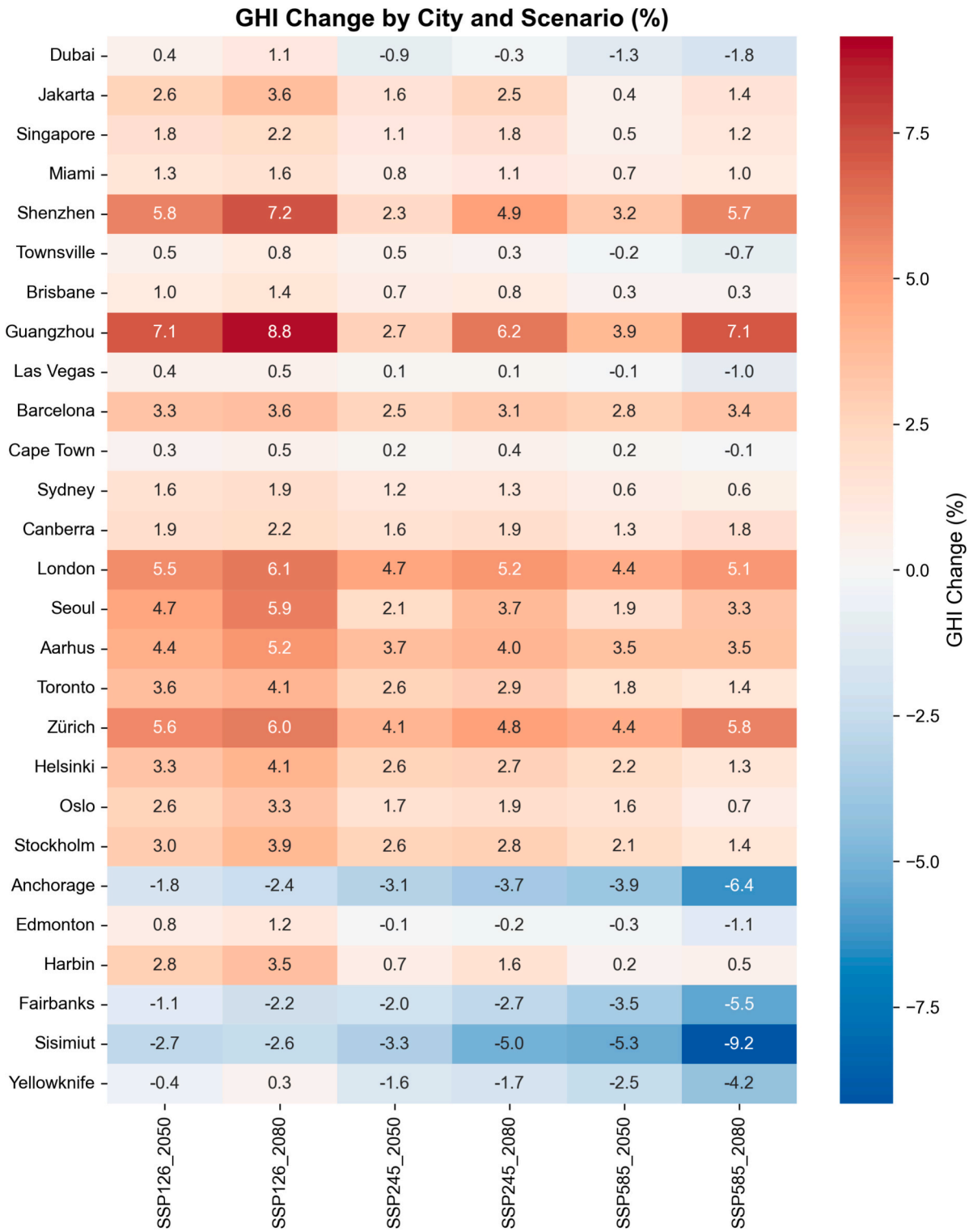


**Fig. 2.** Projected changes in global horizontal irradiation (GHI) by city and scenario relative to baseline.

relationship with climate severity, ranging from 85.0 kWh/m$^2$ in Brisbane and Townsville to 192.0 kWh/m$^2$ in Sisimiut. Cold regions (Zones 6–8) show higher consumption driven by heating requirements, while energy composition varies systematically. Zone 0 cities derive 26.8–31.7% from cooling with negligible heating, Zone 1 cities require 16.1–17.2% cooling, and Zones 5–8 are heating-dominated (40.5–52.4%) with minimal cooling needs (0.2–2.8%). This relationship underscores the climate-specific conditions that building-PV systems must accommodate. To ensure reliability of simulation results, modeled EUI values were compared against ANSI/ASHRAE/IES Standard 100–2018 for energy efficiency in existing buildings [51]. For Miami (ASHRAE Zone 1), the modeled EUI of 85.0 kWh/m$^2$ closely aligns with the standard target of 319 MJ/m$^2$ (88.6 kWh/m$^2$) site energy for single-family detached buildings, representing a −4.1% deviation. Similarly, for Toronto (ASHRAE Zone 5A), the modeled EUI of 143.4 kWh/m$^2$ closely matches the target of 519 MJ/m$^2$ (144.2 kWh/m$^2$), with

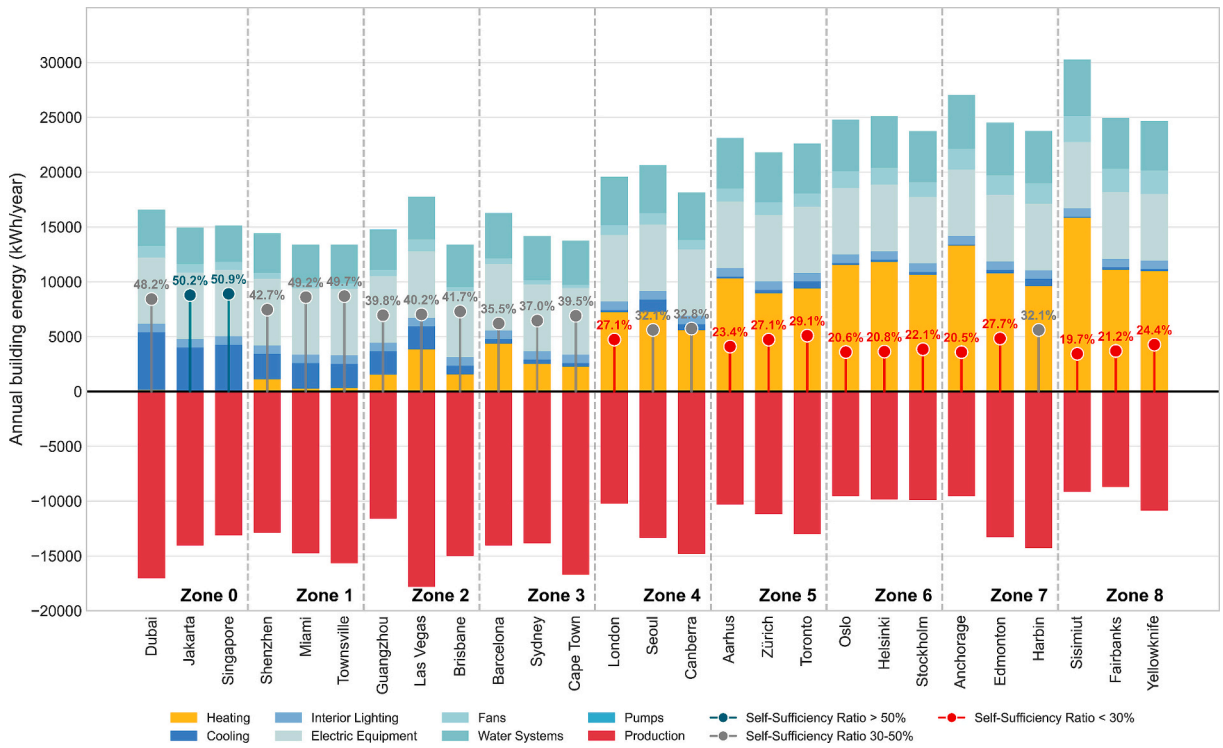


**Fig. 3.** Baseline annual building energy consumption, PV production and self-sufficiency ratio for 27 cities.

a −0.5% deviation. For Anchorage (ASHRAE Zone 7), the modeled EUI of 171.6 kWh/m$^2$ (617.7 MJ/m$^2$) falls within an acceptable range compared to the target of 676 MJ/m$^2$ (187.8 kWh/m$^2$), representing a −8.6% deviation. These comparisons demonstrate reasonable model accuracy across all validated zones, with deviations within acceptable ranges. Notably, even within the same ASHRAE zones, energy consumption can vary considerably. For example, within Zone 3 subcategories (3A, 3B, 3C), the Standard 100–2018 targets range from 250 to 376 MJ/m$^2$ (69.4 to 104.4 kWh/m$^2$), reflecting this intra-zonal variability.

For extreme climate zones where Standard 100–2018 coverage is limited, we validated against additional sources. When comparing cooling energy specifically, Mohammed et al. [52] reported cooling loads of 34.9 kWh/m$^2$ for a base case low-rise residential building in Dubai. Our modeled cooling energy for Dubai is 33.3 kWh/m$^2$ at baseline, representing a 4.8% lower value. For subarctic Zone 8, our modeled values (Sisimiut: 192.0 kWh/m$^2$, Fairbanks: 158.3 kWh/m$^2$, Yellowknife: 156.4 kWh/m$^2$) reflect extreme heating requirements consistent with polar construction practices. In arctic and subarctic regions particularly, weather conditions can differ substantially despite identical zone classifications, contributing to energy performance variations. Variations reflect differences in local weather patterns, specific building design details, envelope thermal performance and HVAC system characteristics across different contexts, confirming that our results fall within acceptable ranges for building energy modeling practice.

PV production generally decreases from warmer to colder regions but with several notable exceptions. For PV yield, baseline specific yield was benchmarked against two established independent reference tools across all 27 study cities: PVWatts v8 (NREL) for North American cities and PVGIS v5.3 for the remaining cities, using the same photovoltaic modeling assumptions for system loss, capacity, and tilt (Supplementary Table S4). Because each reference tool uses its own solar resource dataset rather than the simulation EPW, this comparison is a plausibility check rather than a controlled validation. The mean absolute deviation across all 27 cities is 4.3%, with 25 of 27 cities falling within ±10%. No consistent directional bias is observed across climate zones. These results confirm that the simulated PV yields are physically plausible, and that the cross-climate patterns reported in this study are not artifacts of the PV modeling chain. The highest production occurs in Las Vegas (17,823 kWh/year under baseline), while cold regions typically show the lowest output (8696 kWh/year in Fairbanks). Of particular interest, Harbin and Edmonton demonstrate strong PV production (14,271 and 13,286 kWh/year, respectively) despite their northern latitudes (45.93°N and 53.57°N). This performance reflects favorable solar radiation conditions. These findings underscore that temperature-based climate zone classification is not necessarily consistent with PV performance, as thermal zones capture heating and cooling requirements but do not account for solar resource availability. Continental versus maritime climate characteristics, cloud cover patterns and atmospheric clarity could substantially influence solar resource availability. This intra-zonal variability emphasizes the importance of location-specific assessments even within the same thermal climate classification.

Annual self-sufficiency metrics establish critical reference points for evaluating climate change impacts and reveal a pronounced climate gradient. Zone 0 cities achieve the highest values (Singapore: 50.9%, Jakarta: 50.2%, Dubai: 48.2%), progressively declining through temperate regions (Barcelona: 35.5%, London: 27.1%) to minimal subarctic performance (Sisimiut: 19.7%, Fairbanks: 21.2%), with notable exceptions for Edmonton (27.7%) and Harbin (32.1%). This threefold variation demonstrates fundamental climate-dependent limitations: while PV systems in hot climates approach meeting half of building energy consumption, cold climate applications achieve only one-fifth of demand despite identical system capacities.

### 3.3. Climate change impact assessment

Understanding PV performance under climate change requires analysis at multiple temporal scales, as each reveals distinct aspects of system behavior and resilience. Annual metrics establish energy balance trends, monthly patterns reveal seasonal mismatches, and daily extremes determine real-world system viability.

### 3.3.1. Annual changes in energy consumption across zones

Fig. 4 illustrates the annual changes in building energy performance. Zones 0–5 generally exhibit positive PV output changes (up to +7.2%), while zones 7–8 show negative impacts. Notable increases include Jakarta (+4.0% to +7.2%), Shenzhen and Guangzhou (+5.0% and +6.3% under SSP126_2080), and London (+2.1% to +4.8%). Conversely, high-latitude regions experience substantial decreases: Anchorage (−13.7% to −6.4%), Fairbanks (−12.6% to −5.4%) and Sisimiut (−13.9% to −4.9%). This aligns with the previous study by Jerez et al. [30], who reported that future PV output changes ranged from −14% to 2% in Europe, with decreases of 10–12% in Scandinavian regions. This spatial heterogeneity reflects the solar radiation patterns established in Section 3.1. A particularly noteworthy observation is that notable variations exist even within the same climate zone where cities display contrasting responses, highlighting the importance of local climate factors beyond broad zonal classifications. This increasing trend for London is consistent with Burnett et al. [53], who reported that solar energy resources in southern and southwestern UK are projected to increase under climate change. Specifically, the UK is expected to witness an overall annual increase of 3.6% by the 2050s, rising to 4.4% by the 2080s under high emissions scenarios using UKCP09 probabilistic projections. While the multi-model ensemble approach reduces uncertainties associated with individual GCM biases [46], several sources of uncertainty remain in future climate projections. These include downscaling methodology choices (statistical and dynamical), temporal period selection, baseline weather selection, and emission scenario uncertainty beyond the SSP scenarios examined.

Building total EUI exhibits a clear relationship with climate zones under warming conditions. In general, hot regions face escalating energy demands while cold regions experience decreasing consumption. Extremely hot Zone 0 cities reveal substantial consumption increases (11.7–38.5%): Jakarta (16.1–38.5%) and Dubai (11.7–33.6%). Conversely, cold climate cities show substantial consumption decreases: Helsinki (8.4–19.5%), Aarhus (6.8%–15.1%) and Oslo (6.5%–14.1%), driven primarily by reduced heating demands that outweigh modest cooling increases. Zones 5–6 exhibit reductions ranging from 11.3% to 19.5% under SSP585_2080. This pattern aligns with previous findings [15,16]. Specifically, Jalali et al. [15] demonstrated decreased thermal loads in cold regions but increases in warm zones under RCP scenarios. Zones 2–3 represent a critical transitional threshold between these opposing trends: Brisbane experiences net increases in total EUI (0.3–3.4%), whereas Barcelona shows modest decreases (−5.0% to −3.7%) across all SSP scenarios, indicating transitional climate behavior under warming scenarios.

Fig. 5 shows a more detailed analysis of how heating and cooling shifts under climate change. Zone 0 cities experience severe annual cooling increases of 102–132% under SSP585_2080: Singapore (27.0 to 60.5 kWh/m$^2$), Dubai (33.3 to 67.3 kWh/m$^2$) and Jakarta (25.4 to 58.9 kWh/m$^2$), while minimal heating energy is essentially eliminated. These results indicate compounding vulnerabilities as cooling demands

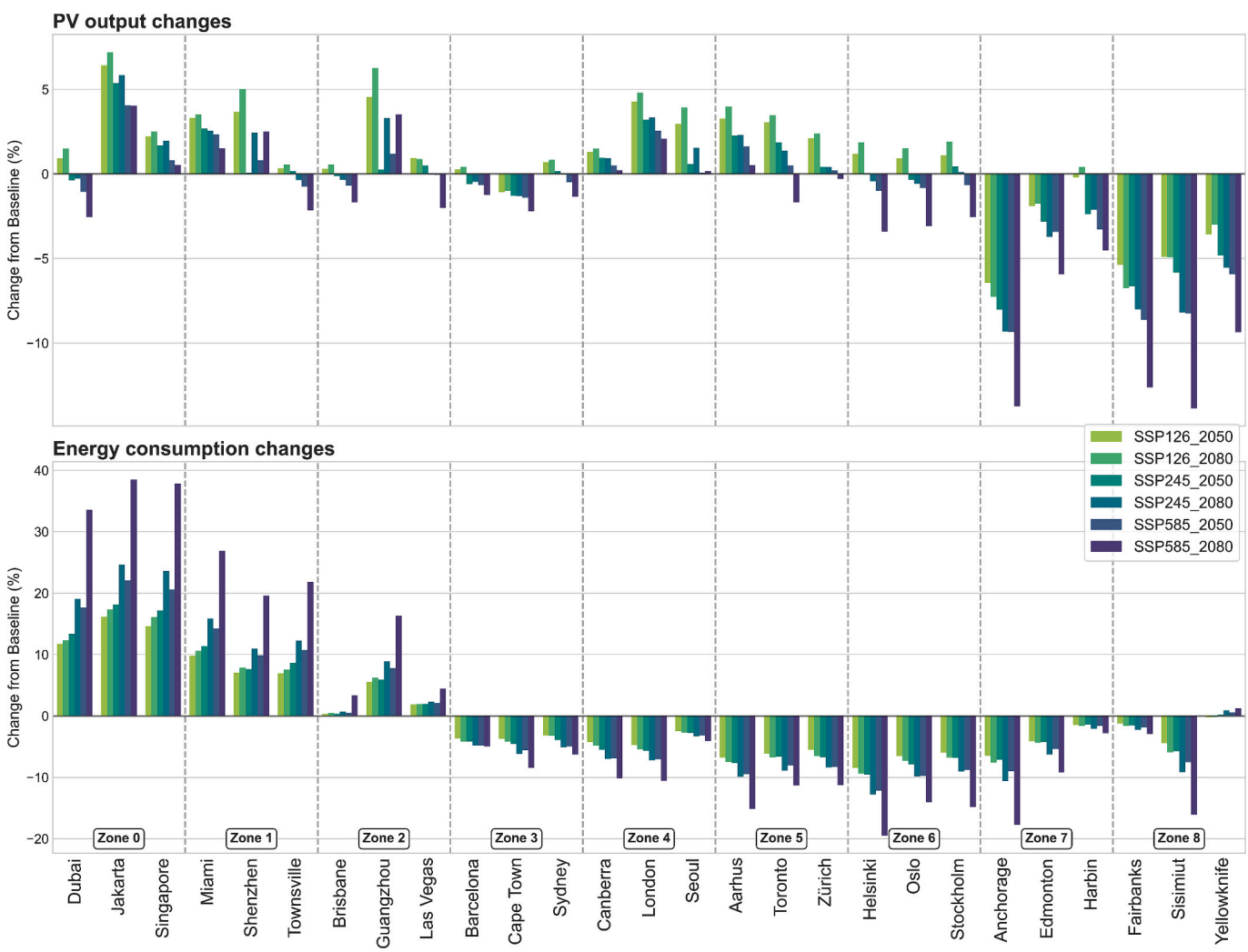


**Fig. 4.** Annual percentage changes in PV generation and energy consumption relative to baseline.

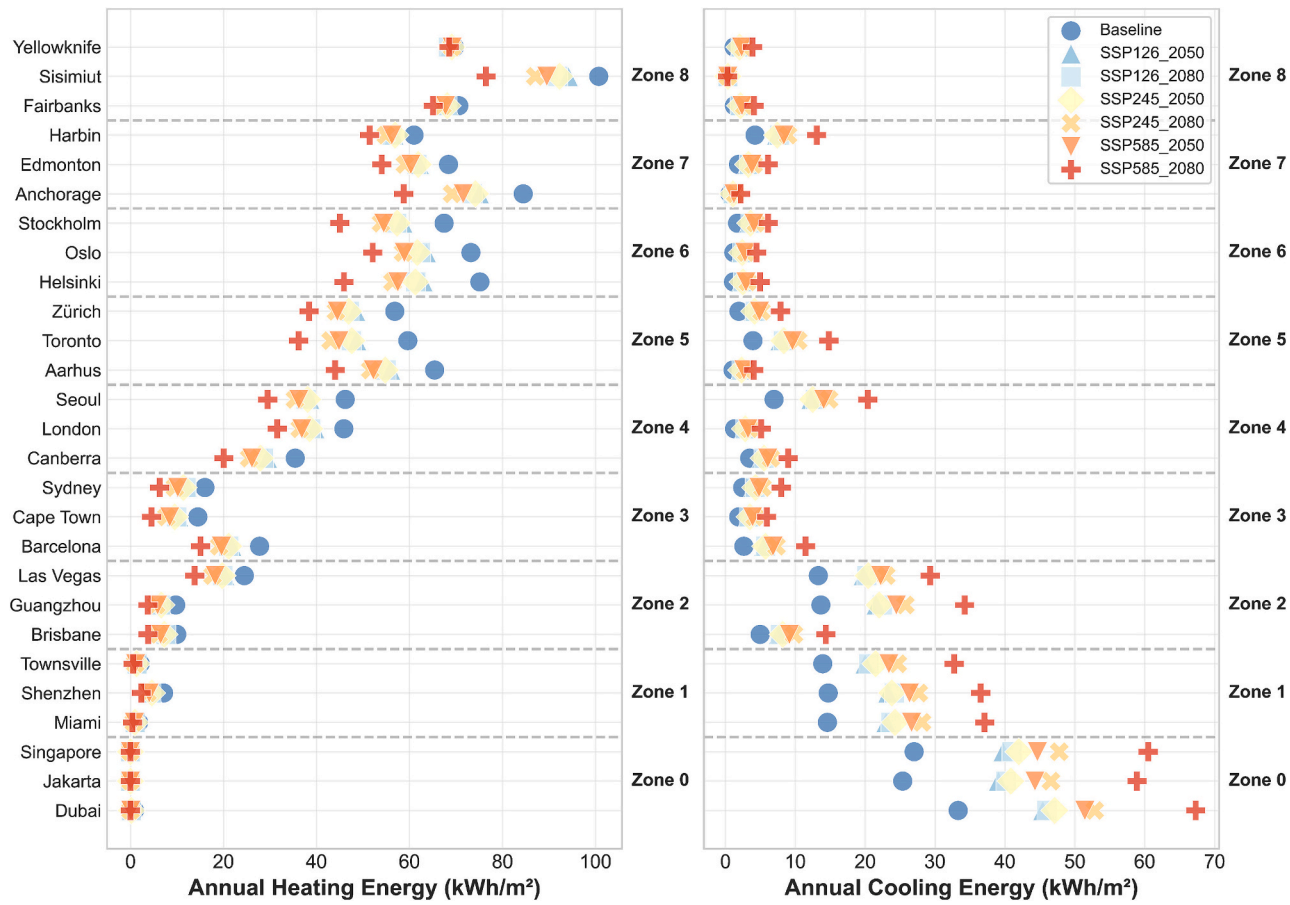


**Fig. 5.** Annual heating and cooling energy consumption by city and scenario.

escalate and HVAC efficiency typically decreases with rising outdoor temperatures as highlighted by [16,54]. However, notable uncertainty exists regarding future technological trajectories and their implications for energy projections. Two opposing forces create complex scenarios. Technological advancement presents substantial mitigation potential. Barea et al. [55] showed that COP increased from 2.3 (current) to 4.4 by 2090 might reduce cooling demands below current levels despite warmer temperatures. Conversely, building envelope aging and system performance (HVAC/PV) degradation over time [56,57], could worsen projected energy balance conditions. The interaction between technological advancement and system degradation represents a critical uncertainty that could significantly influence future building energy performance. This technological-degradation dynamic varies substantially across regions with different economic development levels, climate conditions and policy frameworks, highlighting the importance of considering both enhancement potential and infrastructure limitations in long-term energy planning strategies.

Transitional climate zones (2–3) demonstrate the most pronounced transformation in thermal energy composition, with multiple cities transitioning from heating-dominated to cooling-dominated profiles. The heating/cooling ratio for Brisbane shifts from 2.0 at baseline to 0.3 under SSP585_2080, while Las Vegas undergoes a similar transformation from 1.8 to 0.5. This fundamental recharacterization represents a critical design threshold requiring substantial HVAC system adaptation. The divergent net energy outcomes despite similar compositional shifts highlight the complex interplay between reduced heating and increased cooling demands in temperate regions.

Climate zones (4–8) exhibit significant heating energy reductions that outweigh absolute increases in cooling demands, resulting in net thermal energy savings. Helsinki demonstrates dramatic heating demand reduction from 75.1 to 45.9 kWh/m$^2$ (38.9% decrease) under SSP585_2080, while Stockholm's heating falls from 67.4 to 45.0 kWh/m$^2$ (33.2% decrease). Despite substantial percentage increases in cooling energy (Helsinki: +332%, Oslo: +272%), absolute values remain minimal compared to heating demands (Helsinki: 1.1 to 5.0 kWh/m$^2$). Net thermal energy reductions vary considerably across cold climate zones, with Zone 6 showing substantial decreases of 19.5% for Helsinki, 14.1% for Oslo, and 14.8% for Stockholm under SSP585_2080.

Harbin (Zone 7) presents a different thermal transition situation compared to maritime Scandinavian cities. While heating demands decrease from 61.0 to 51.4 kWh/m$^2$ (15.7% reduction) under SSP585_2080, cooling demands increase dramatically from 4.2 to 13.1 kWh/m$^2$ (208.7% increase). Critically, the absolute magnitudes of heating reduction (9.6 kWh/m$^2$) and cooling increase (8.9 kWh/m$^2$) are nearly equivalent, resulting in minimal net thermal energy savings. This pattern contrasts sharply with Scandinavian maritime cities (Helsinki, Oslo and Stockholm) where heating reductions (up to 30 kWh/m$^2$) substantially exceed cooling increases (3–5 kWh/m$^2$). Harbin's near-equilibrium demonstrates that continental interior locations may experience fundamentally different climate transitions than coastal cities at similar latitudes, with more pronounced summer warming driving substantial cooling loads while winter temperature moderation remains modest.

In Subarctic Zone 8, variability intensifies further. Yellowknife demonstrates a slight heating reduction (69.6 to 68.5 kWh/m$^2$; 1.6% decrease), while Sisimiut exhibits a pronounced decrease (100.7 to 76.4 kWh/m$^2$; 24.1% decrease). This variability highlights considerable climate sensitivity differences within polar regions, likely reflecting local warming patterns and geographic factors such as maritime versus continental influences. Importantly, heating demands continue to

dominate in severe cold regions, with cooling representing less than 5% of total HVAC energy even under SSP585_2080. This persistence indicates that while warming provides energy benefits in most cold climates, it does not fundamentally alter the underlying thermal characteristics that define these regions, though continental interior cities like Harbin may experience compounding heating-cooling transitions requiring dual-season adaptation strategies.

Global warming significantly alters the temporal relationship between PV output and building energy demand, creating pronounced regional divergences in energy balance performance (Fig. 6). Hot climate Zones (0–1) experience progressive energy balance (Production-Consumption) deterioration under warming scenarios. Jakarta demonstrates severe degradation from −901 kWh baseline to −6085 kWh under SSP585_2080 (575% increase), while Dubai exhibits even more dramatic deterioration from 463 kWh to −5534 kWh. These deficits highlight the substantial challenges in addressing the surge in energy requirements in tropical climates. This deficit intensifies with both scenario severity and time horizon, with SSP585_2080 consistently producing the most extreme impacts. Several Zone 1–2 cities exhibit critical threshold transitions from energy surplus to deficit under climate change. Miami exemplifies this vulnerability, with its energy balance deteriorating from +1372 kWh/year (baseline) to +471 kWh (SSP126_2080), −379 kWh (SSP245_2080) and −2005 kWh (SSP585_2080). Townsville and Las Vegas follow similar trajectories, crossing from baseline surpluses (+2262 and +64 kWh/year respectively) into deficits under SSP585_2080 (−994 and −1075 kWh/year). This complete reversal from net energy producers to consumers creates a new category of climate-vulnerable locations requiring proactive

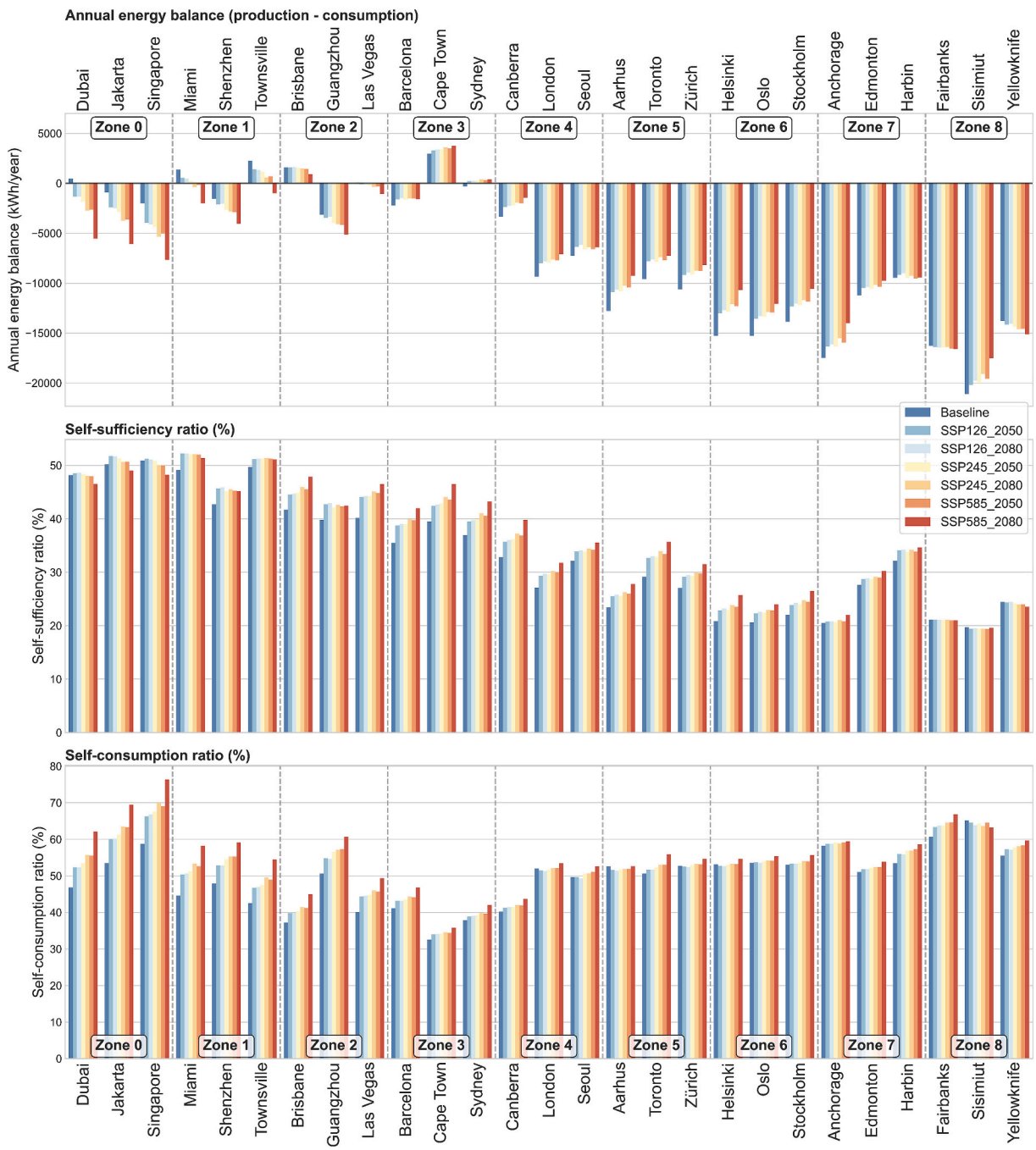


**Fig. 6.** Annual building energy balance (generation minus demand), SSR and SCR under climate change.

interventions (increased PV capacity, storage integration or demand reduction measures) to maintain current performance levels. Conversely, cold regions (Zones 6–8) experience substantial energy balance improvements under warming conditions, most notably in Helsinki (−15,259 kWh to −10,703 kWh, a 30% reduction) and Aarhus (−12,791 kWh to −9250 kWh, a 28% reduction). This divergent response creates a marked gap in energy resilience between hot and cold regions under global warming.

To better understand on-site energy utilization, SSR and SCR are analyzed. Extremely hot climate cities (Zone 0) experience consistent SSR deterioration despite having the highest baseline values. Singapore's SSR declines from 50.9% to 48.2% under SSP585_2080, while Dubai decreases from 48.2% to 46.5%. This decline reflects rising cooling demands outpacing modest PV generation gains in Singapore, further exacerbated by production reduction in Dubai. Interestingly, moderately hot and temperate zones demonstrate systematic SSR improvements. Miami increases from 49.2% to 51.4%, and Cape Town from 39.5% to 46.5% under SSP585_2080. Cold regions show accelerating improvements under severe warming scenarios, creating paradoxical outcomes where extreme climate change produces favorable PV performance from an annual energy balance perspective.

SCR increases consistently across all climate zones, with the most dramatic changes in hot regions. Singapore demonstrates a steep progression from 58.7% to 76.3%, while Jakarta increases from 53.5% to 69.4% under SSP585_2080. This trend indicates enhanced temporal alignment between increased daytime cooling demands and solar availability. Cold regions exhibit more modest SCR impacts. Fairbanks shows a constrained response (60.7% to 66.8%), representing approximately one-third of the magnitude of tropical changes. This reflects the combination of slight cooling increases and heating reductions (predominantly during non-solar hours), resulting in limited influence on daytime consumption profiles.

The complex interaction between these metrics reveals how climate change fundamentally reshapes the potential for PV integration. Cape Town (Zone 3) and Brisbane (Zone 2) emerge as remarkably climate-resilient locations, maintaining positive energy balances across all warming scenarios. Cape Town demonstrates an improved energy balance from 2951 kWh (baseline) to 3744 kWh under SSP585_2080, while Brisbane shows SSR improvement from 41.7% to 47.9%. This resilience stems from a critical equilibrium in heating/cooling load balance that distinguishes transitional zones from extreme climates.

Transitional zones begin with moderate heating loads (Cape Town: 14.5 kWh/m$^2$ heating vs 1.9 kWh/m$^2$ cooling; Brisbane: 9.9 vs 5.0 kWh/m$^2$) occurring predominantly during non-solar hours. Climate warming delivers substantial heating reductions (Cape Town: 68.9% decrease to 4.5 kWh/m$^2$; Brisbane: 62.0% decrease to 3.8 kWh/m$^2$) that directly improve energy balance without compromising PV utilization. Meanwhile, cooling increases remain moderate: Cape Town rises only 4.0 kWh/m$^2$ (to 5.9 kWh/m$^2$) while Brisbane increases 9.4 kWh/m$^2$ (to 14.4 kWh/m$^2$). Cape Town achieves net thermal energy savings, while Brisbane's net increase remains minimal. Most critically, this shift toward balanced heating/cooling profiles improves temporal matching, as daytime cooling loads align favorably with peak solar production while reduced heating eliminates evening demand peaks.

This balanced response contrasts sharply with extreme zones. Hot regions (Zones 0–1) lack offsetting heating reductions, minimal baseline heating provides negligible buffer against surging cooling demands (Singapore increases by 33.5 kWh/m$^2$), creating pure demand escalation and systematic energy balance deterioration. PV generation becomes increasingly inadequate despite being more fully utilized. Conversely, cold regions (Zones 6–8) achieve substantial heating reductions (Helsinki decreases by 29.2 kWh/m$^2$) but astronomical constraints limit winter PV generation regardless of warming. Transitional zones thus represent optimal climate conditions where moderate baseline temperatures enable both meaningful heating reductions and year-round solar resource availability, creating favorable conditions for climate-adaptive renewable energy integration.

These findings also emphasize the need for climate-specific adaptation strategies, particularly enhanced storage capacities and optimization of PV system sizing in hot climates to counteract the climate-induced degradation in renewable energy integration potential. Recent research demonstrates that innovative system configurations can improve performance outcomes. Krarti [58] investigated rotating PV systems and housing units, reporting that substantial energy demand reductions occur when using rotating housing equipped with independently controlled rotating rooftop PV systems. These findings highlight optimization potential through dynamic tilt angle adjustment and rotation mechanisms that enhance both PV output capacity and solar resource utilization. However, practical implementation faces substantial economic constraints that limit widespread adoption of optimal configurations. Ren et al. [59] stated that Australian rooftop installations typically utilize existing roof angles (15–22.5 degrees) because tilt frame costs consistently exceed financial benefits. Specifically, it is more economical to simply add 1–2 additional solar panels to increase overall system capacity. This economic reality creates tension between pursuing maximum technical efficiency in PV systems and maintaining cost-effective deployment in real-world applications. Energy storage systems represent another critical component for enhancing PV resilience, particularly under extreme weather conditions. Storage integration can significantly mitigate solar integration risks while reducing the probability of catastrophic blackouts during extreme events [36].

Hot climate PV systems, particularly those in Zone 0–1 cities, should prioritize multiple efficiency improvement pathways to maintain current self-sufficiency levels under increasing thermal stress. These improvements should encompass advanced building envelope retrofits to curb cooling surge, enhanced PV module cooling strategies, and integration of smart building energy management systems that optimize load scheduling to align with peak PV generation periods. Conversely, cold climate cities require comprehensive renovation strategies that address both declining heating loads and emerging cooling demands, despite the overall beneficial trend in net thermal energy reduction.

Fig. 7 presents annual grid exchange patterns, revealing systematic reductions in surplus electricity exports across all climate zones with pronounced geographic variations. Hot regions experience substantial export reductions, with Jakarta declining 31.7% (6534 to 4465 kWh) and Dubai decreasing 30.4% (9055 to 6300 kWh) under SSP585_2080. Similar patterns extend across Zones 1–2, with reductions ranging from 13.7% to 23.5% for the same scenario. Conversely, temperate and cold regions demonstrate greater resilience, with export reductions typically below 15% in Zones 4–6, while some cities even increase (Aarhus: 0.4% to 6.5%; Seoul: −5.8% to 4.5%; Zurich: −4.4% to 3.1% for all SSP scenarios).

Regarding electricity imports from the utility grid, climate zones (0–2) universally experience substantial increases in grid electricity imports under warming scenarios, with the most severe intensification observed in Zone 0. However, temperate and cold regions demonstrate consistent reductions in grid electricity imports. For instance, London shows a reduction from 14,274 kWh in baseline to 11,958 kWh in SSP585_2080 (16.2% decrease), and Stockholm from 18,499 kWh to 14,861 kWh (19.7% decrease).

These regionally differentiated energy performance outcomes have profound implications for global energy security and public health, particularly when considered alongside population distribution patterns and infrastructure vulnerability. While extremely cold regions (Zones 7–8) demonstrate favorable PV performance improvements under warming scenarios, these areas typically represent relatively sparse population densities compared to the tropical and subtropical zones experiencing the most severe energy balance deterioration. The concentration of global population in hot climate regions fundamentally magnifies the adverse implications of deteriorating PV performance, as cities such as Singapore and Jakarta experience substantial cooling

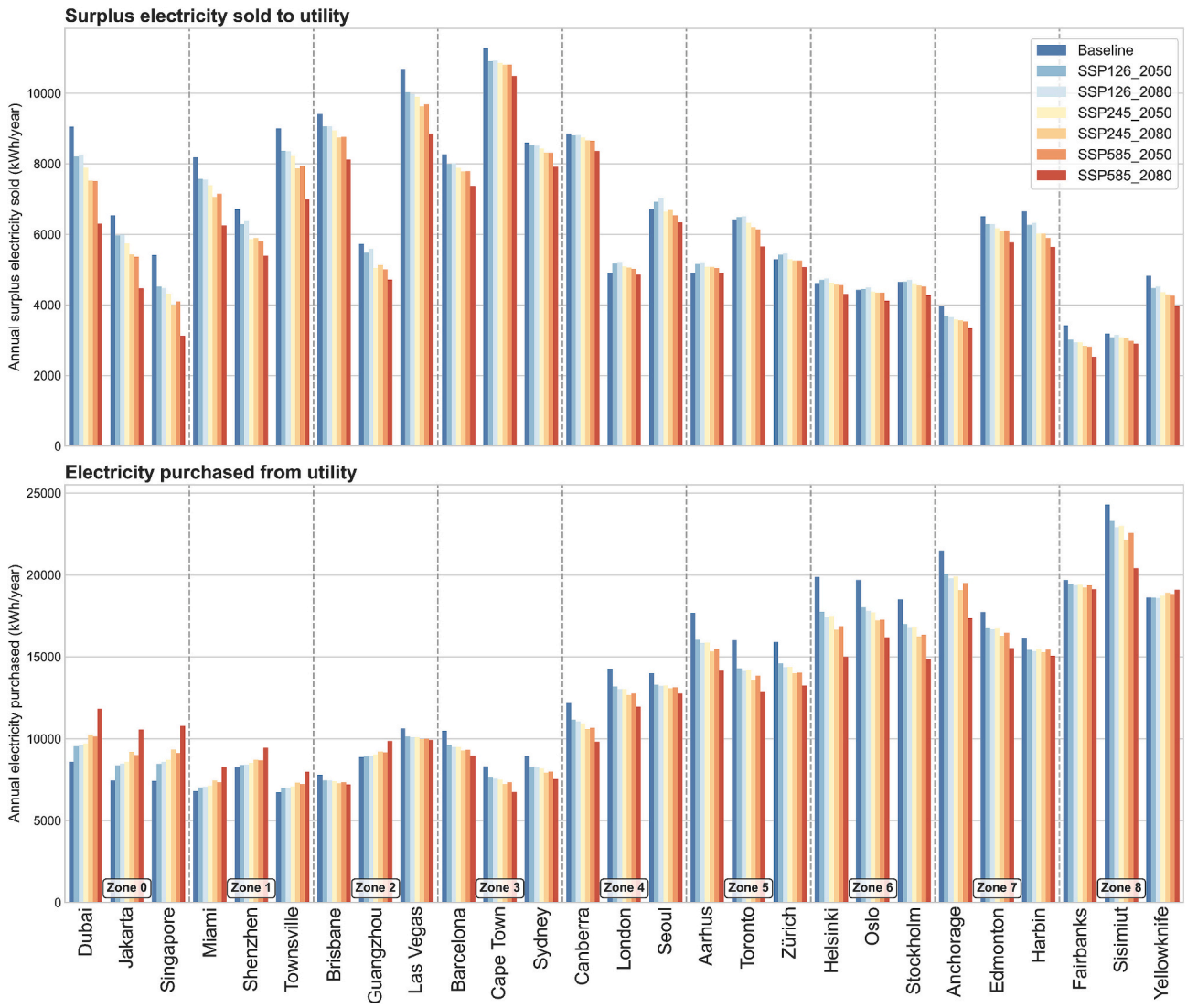


**Fig. 7.** Annual electricity exports to and imports from the grid by climate zone.

energy surges coinciding with declining renewable self-sufficiency. The Asia-Pacific region, encompassing many Zone 0–1 cities, houses approximately 60% of the global population [60], meaning that the observed 6.9–38.5% increases for SSP scenarios in total EUI affect billions of people. As demonstrated by Mutschler et al. [61], while climate change reduces Swiss heating demands, population growth largely compensates for these energy savings. This demographic asymmetry creates unprecedented stress on electrical distribution networks through the compound effect of increasing cooling demands and declining renewable generation capacity in population-dense hot regions. Most importantly, it poses critical risks to public health and economic stability in regions where billions depend on reliable electricity access for thermal comfort and essential services.

Beyond immediate grid stability, these divergent energy performance trajectories have notable implications for operational carbon emissions, though quantifying these emissions impacts introduces substantial methodological complexity. Building operational emissions depend critically on the interplay between energy demand patterns, fuel sources, electricity grid carbon intensity and the contribution of on-site renewable generation. If electricity grid emissions factors remain constant and on-site PV interactions are not considered, emissions trends would mirror total energy consumption patterns. Previous studies demonstrate divergent emissions outcomes across climate zones [40,45]. Ciancio et al. [40] showed that in cold regions such as Copenhagen and Gothenburg where heating is dominant, total emissions tend to decrease due to substantial heating reduction. However, in Granada and Palermo, the surge in cooling coupled with higher emissions coefficients leads to increasing GHG emissions. In a Canadian study, Berardi and Jafarpur [62] found that future emissions across all 16 prototype buildings are projected to decrease, attributed to the lower carbon intensity of cooling (0.036 kg/kWh of electricity) compared to heating (0.180 kg/kWh of natural gas). This occurs because reducing heating favors GHG emissions reduction, while increases in cooling contribute relatively small amounts of emissions due to the large renewable energy contribution to the grid.

However, incorporating on-site PV generation substantially complicates emissions accounting. The emissions benefits of PV depend on whether generated electricity displaces grid consumption (avoiding emissions) or is exported to the grid (potentially displacing marginal generation sources with different emissions intensities). Our findings that hot regions experience declining SSR and increasing grid imports suggest an increased emissions burden under climate change, as buildings increasingly rely on grid electricity during periods of high cooling demand. Conversely, cold regions with improving energy balances may achieve greater emissions reductions as PV offsets larger fractions of building loads. Critical to accurate emissions assessment is the use of

dynamic emissions factors rather than static average values [63,64]. Amaripadath et al. [63] demonstrated that static factors can lead to 111% underestimation (Paris) or 120% overestimation (New York) of annual operational emissions intensity compared to dynamic grid emission factors. Since PV generation peaks during midday while building loads vary greatly across climate conditions, the emissions benefits vary substantially by location and time period.

Furthermore, future energy mix evolution introduces fundamental uncertainty into emissions projections, as decarbonization pathways vary substantially across regions and policy contexts. Modeling electricity emissions in alignment with climate models and scenarios could improve the reliability of operational emissions projections [65]. Policy shocks and extreme events can further alter assumed trajectories, as demonstrated by increased emission factors in Japan following the Fukushima nuclear accident [66], highlighting the difficulty of projecting long-term emissions benefits. These complexities underscore that while the study documents the future energy performance, reliable emissions projections require explicit modeling of future grid transformations beyond our current scope.

### 3.3.2. PV-consumption matching monthly analysis

This section examines monthly variations in PV performance metrics across representative city profiles, with additional city-specific data provided in SM (Fig. S1–27). To facilitate direct comparison, PV production is normalized by building gross floor area (kWh/m$^2$). Hot regions (Zones 0–2) benefit from peak cooling demand coinciding with maximum solar availability, creating favorable conditions for direct PV consumption. Conversely, cold regions (Zones 6–8) experience substantial temporal mismatches where peak energy demands occur during winter months when PV production reaches minimum levels due to reduced solar radiation and limited daylight hours. This disparity explains the decreasing SSR observed in progressively colder climates and highlights the fundamental challenge for PV implementation in heating-dominated regions.

Zone 0 cities demonstrate stable year-round PV generation patterns, maintaining monthly SSR values of 40.0–55.8% under baseline conditions. However, analysis reveals progressive degradation under warming scenarios. Singapore exemplifies this vulnerability, with monthly SSR declining from 46.0–55.8% (baseline) to 43.2–52.9% under SSP585_2080 (Fig. 8a). Deterioration peaks during cooling months in

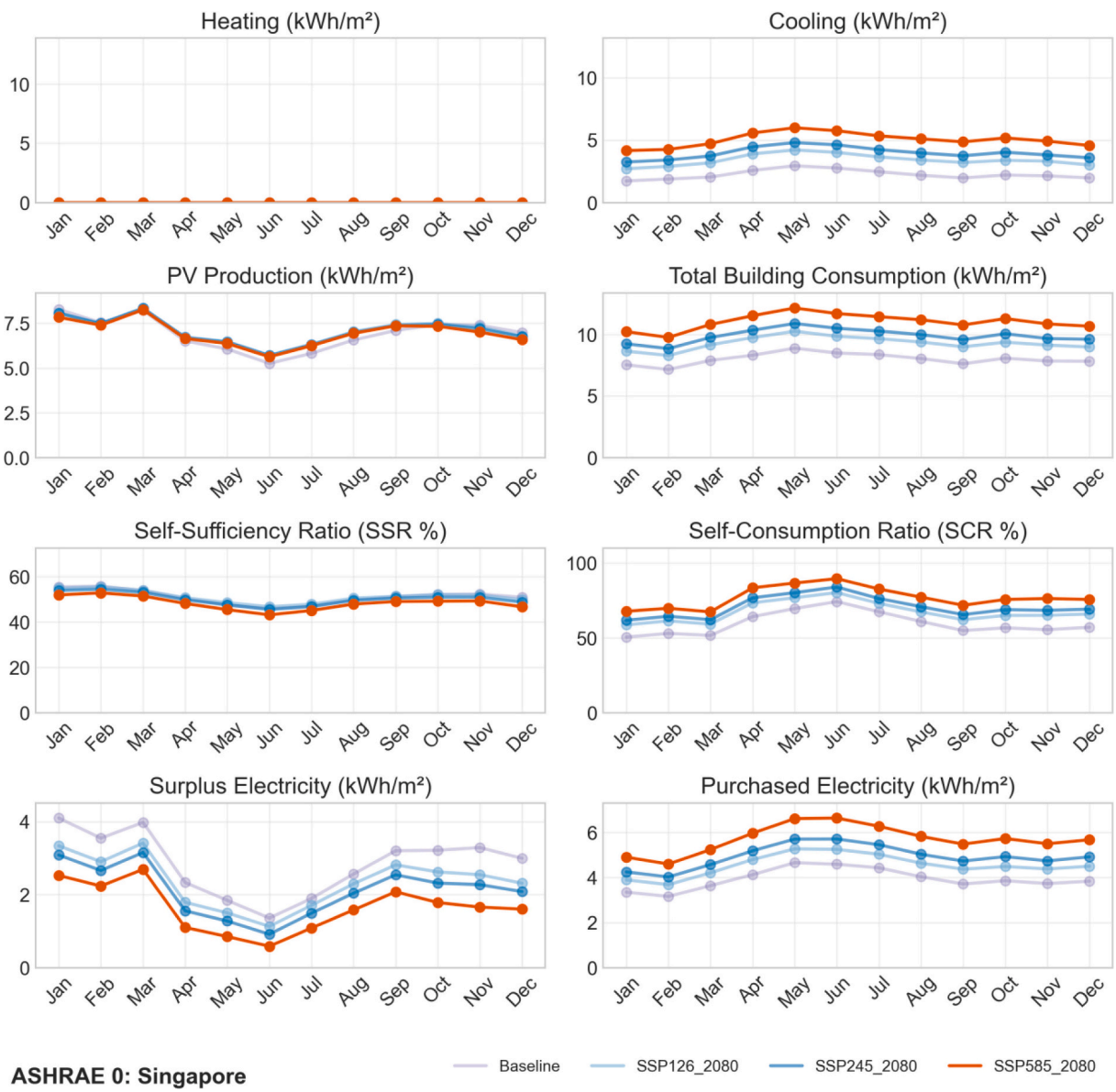


**Fig. 8.** Monthly PV generation, building demand and grid exchange for Singapore (a), Oslo (b) and Cape Town (c).

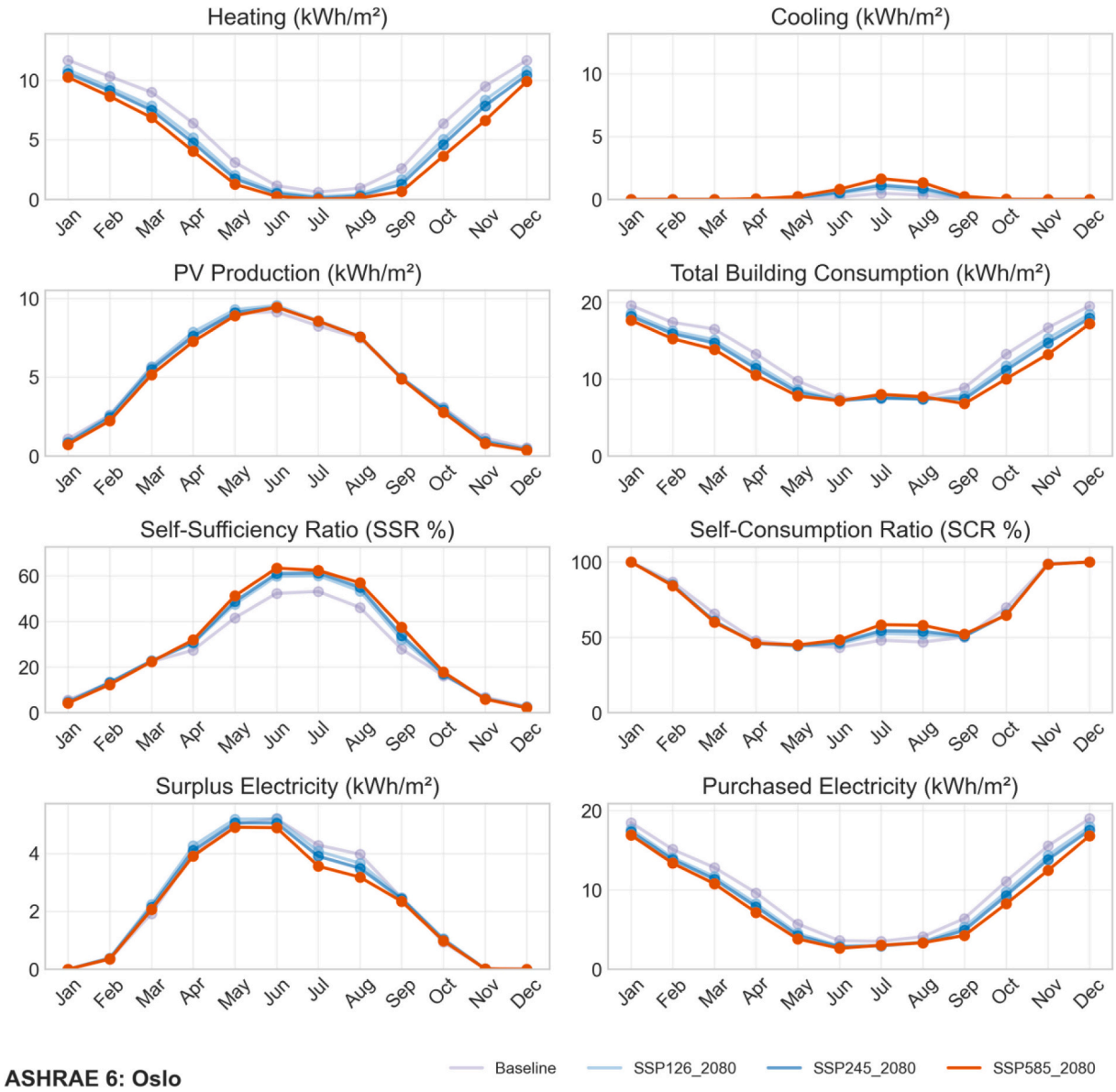


**Fig. 8.** (*continued*).

Dubai (Jul-Aug), where cooling demands nearly double from 6.4–6.6 kWh/m$^2$ to 11.6–12.0 kWh/m$^2$. This non-linear response suggests that existing building envelope designs in extreme hot climates may possess lower resilience. While temporal alignment between peak cooling and solar generation theoretically favors PV integration, cooling surge magnitude overwhelms generation capacity. This phenomenon creates improved temporal matching yet degraded SSR, representing a critical vulnerability for renewable energy systems in thermally stressed regions. Similar patterns emerge across tropical cities: Shenzhen (Fig. S5) and Townsville (Fig. S6) exhibit lower summer SSR values under future scenarios but improved winter performance. Winter improvements result from the virtual elimination of minimal heating loads occurring during non-solar hours. Shenzhen demonstrates this effect with January heating demands decreasing from 2.5 to 1.2 kWh/m$^2$ and December values dropping from 1.7 to 0.5 kWh/m$^2$. This reduction of heating loads improves temporal matching between solar availability and remaining energy demands.

Cold climate regions (Zones 4–8) are characterized by extreme seasonal asymmetry in self-sufficiency despite substantial climatic warming. Oslo (Fig. 8b) exemplifies this persistent constraint, with SSR values ranging from 2.7% (December) to 53.1% (July) under baseline conditions. Despite substantial winter warming, SSR shows no improvement (2.1% in December for SSP585_2080), while summer values moderately increase to 63.4% (June) and 62.4% (July). This extreme seasonal disparity persists even under the severe warming scenario. The analysis demonstrates that astronomical constraints, rather than temperature limitations, constitute the primary barrier to winter renewable energy performance in high-latitude regions.

Transitional climate zones emerge as potentially optimal PV deployment locations, exemplified by Cape Town (Fig. 8c) with the baseline SSR of 27.2–54.8% improving to 32.5–59.4% under severe warming. This consistent performance, coupled with improvements in both SSR and SCR, suggests moderate climate zones with balanced heating and cooling demands may offer the most resilient renewable energy integration conditions. Furthermore, Cape Town undergoes thermal profile transformation: heating dominance from March–November (baseline) reverses to May–October under SSP585_2080. The heating/cooling ratio decreases from 7.6 to 0.8, signifying the complete reorientation of building thermal requirements necessitating fundamental HVAC design reconsideration. The analysis reveals critical

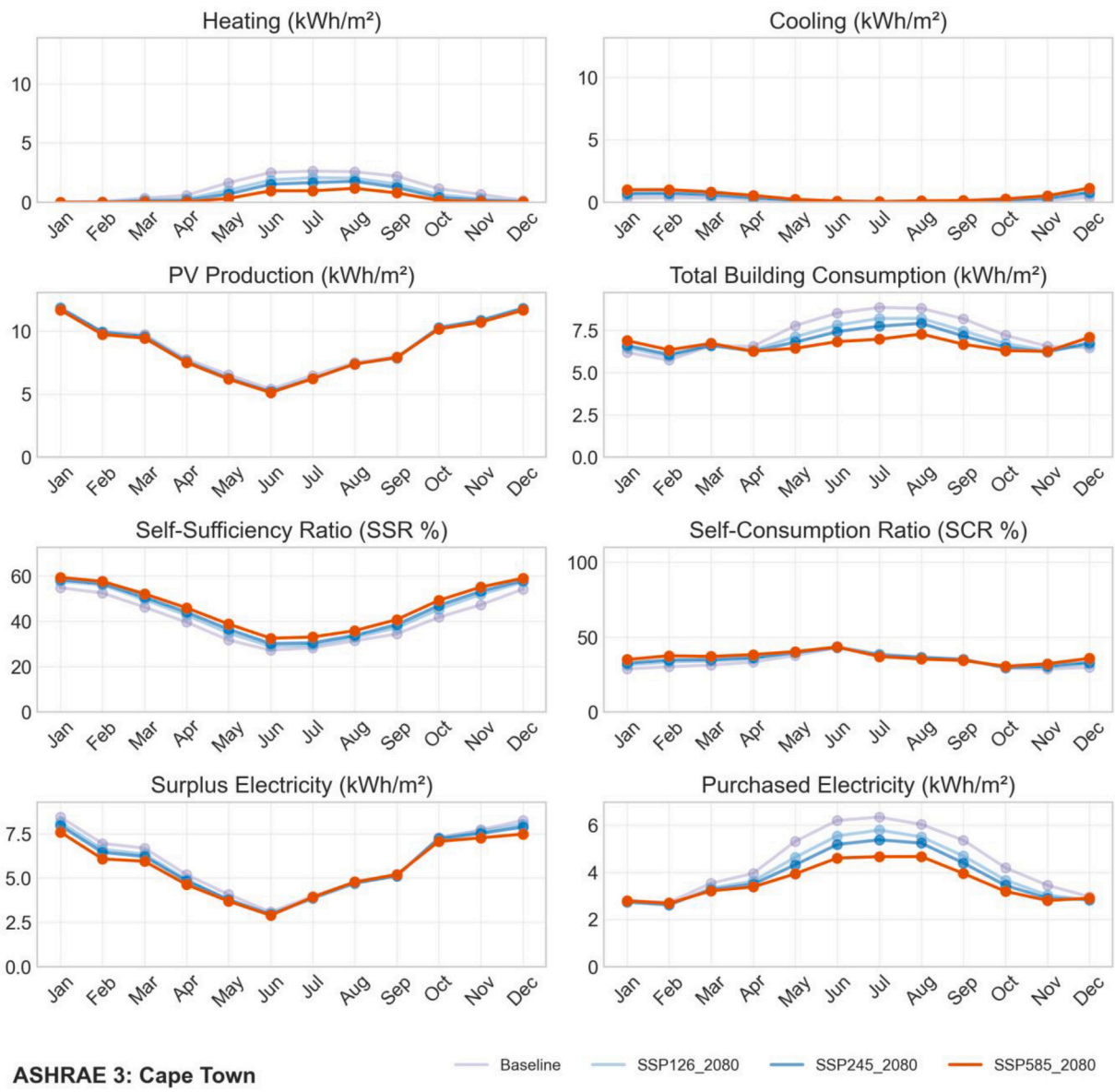


**Fig. 8.** (*continued*).

threshold transitions where specific months shift from heating-dominated to cooling-dominated patterns. However, the absolute values of heating and cooling are still small compared to tropical and cold regions. Sydney (Fig. S12) demonstrates this phenomenon clearly: April heating/cooling loads of 0.65/0.16 kWh/m$^2$ (baseline) transition to 0.11/0.52 kWh/m$^2$ under SSP585_2080, while October shows a similar transformation from 1.31/0.17 kWh/m$^2$ to 0.25/0.56 kWh/m$^2$. These transitions extend cooling system operational periods into spring and autumn months, creating cascading PV performance benefits as daytime cooling demands align more favorably with solar generation than traditional morning/evening heating loads. Consequently, Sydney's April SSR improves from 37.1% (baseline) to 42.7% (SSP585_2080), with October showing similar gains (40.7% to 48.9%). This improvement represents a potentially significant but underexplored benefit of climate warming for renewable energy integration in transitional climate regions.

Monthly grid interaction patterns reveal critical challenges for utility infrastructure planning under climate change. Hot climate regions experience comprehensive deterioration in grid exchange profiles: Singapore's monthly electricity exports collapse from 1.4–4.1 kWh/m$^2$ (baseline) to 0.6–2.7 kWh/m$^2$ under SSP585_2080, while grid purchases surge from 3.2–4.7 kWh/m$^2$ to 4.6–6.6 kWh/m$^2$. Dubai exhibits parallel degradation, with surplus generation declining from 3.1–6.8 kWh/m$^2$ (baseline) to 1.1–5.6 kWh/m$^2$ (SSP585_2080), accompanied by increased grid dependence with monthly imports rising from 3.2–6.8 kWh/m$^2$ to 3.0–10.7 kWh/m$^2$. Specifically, under SSP585_2080, monthly grid purchases increase by up to 57.4% in Dubai (August: 6.8 to 10.7 kWh/m$^2$), 46.2% in Jakarta (March: 3.9 to 5.7 kWh/m$^2$), and 48.6% in Singapore (November: 3.7 to 5.5 kWh/m$^2$). For electricity exports, significant reductions occur: 64.5% in Dubai (August: 3.1 to 1.1 kWh/m$^2$), 40.0% in Jakarta (May: 3.5 to 2.1 kWh/m$^2$), and 57.1% in Singapore (June: 1.4 to 0.6 kWh/m$^2$). This bidirectional deterioration reduces self-sufficiency precisely when cooling demand peaks. Because it persists across all months, seasonal load shifting alone would not close the gap, which points to a structural supply-demand mismatch at the building scale rather than a problem of timing. While technological advances in PV efficiency and expanded system sizing offer potential mitigation, concerns regarding behavioral rebound effects, where efficiency gains stimulate increased consumption, may partially offset these improvements [31,67,68].

Cold climate regions demonstrate contrasting patterns characterized by reduced grid dependence during historically deficit-intensive periods. Stockholm's winter month electricity imports (November–February) decrease from 14.2–17.9 kWh/m$^2$ (baseline) to 11.5–15.6 kWh/m$^2$ under SSP585_2080, creating opportunities for infrastructure optimization (Fig. S21). A particularly concerning trend emerges in the systematic erosion of electricity export capacity across all climate zones, with pronounced impacts during cooling-dominated months. Singapore's SCR escalates from 67.5–74.2% (baseline in May to July) to 82.6–89.6% under SSP585_2080, while Dubai shows similar increase from 62.9–66.2% to 83.0–87.2% during June–August. Such high SCR values indicate that nearly all on-site generation is consumed locally, with little surplus exported, so these systems shift from net exporters toward near-complete self-consumption as cooling demand rises.

The pronounced temporal mismatches revealed by monthly analysis necessitate targeted technological interventions beyond simple capacity expansion, with demand-side strategies often proving more cost-effective than supply-side solutions. In hot climates, the exponential growth in monthly cooling loads highlights the critical importance of building envelope improvements [8,9], including cool or green roofs, dynamic shading systems, and high-performance glazing. These passive measures function as “virtual storage” by reducing the magnitude of supply–demand mismatches rather than attempting to bridge them through physical storage. In cold climates, comprehensive renovation strategies remain essential despite natural heating load reductions. Although cities such as Helsinki, Stockholm, and Oslo experience winter heating demand reductions of up to 40% (e.g., Helsinki in December) under SSP585_2080, winter monthly self-sufficiency ratios persistently remain below 15% (with the exception of Harbin; Fig. S24). This demonstrates that passive benefits from temperature increases alone are insufficient to resolve fundamental temporal mismatches. As shown by D'Agostino et al. [27], NZEBs with high-performance envelopes achieve superior load matching by reducing thermal losses and improving temporal alignment between energy demand and available solar resources, particularly during winter periods characterized by limited solar availability. Such proactive envelope-focused interventions deliver immediate performance benefits while simultaneously mitigating the carbon emissions driving climate change.

The integration of emerging technologies presents both opportunities and challenges. Electric vehicles introduce particular complexity to PV integration, functioning simultaneously as substantial loads and potential grid-supporting resources [69,70]. Without intelligent management, EV charging could exacerbate grid strain during low-production winter months in temperate and cold regions where SSR values already fall below 15%. However, intelligently managed bidirectional charging systems could theoretically provide critical support during deficit periods. Heating electrification amplifies challenges by substantially increasing winter electricity demand precisely when PV production reaches minimum levels in high-latitude regions. These considerations establish that electrification transitions must incorporate complementary strategies rather than relying exclusively on PV generation.

### 3.3.3. *Thermal performance under extreme climate events*

While annual energy balances provide valuable baseline metrics, they mask critical hourly temporal mismatches that determine system resilience. By examining hottest and coldest 3-day profiles (Fig. 9), this section reveals the practical limitations of PV systems, identifies system vulnerabilities and highlights implications for grid infrastructure resilience during critical periods. The variability in extreme event dates

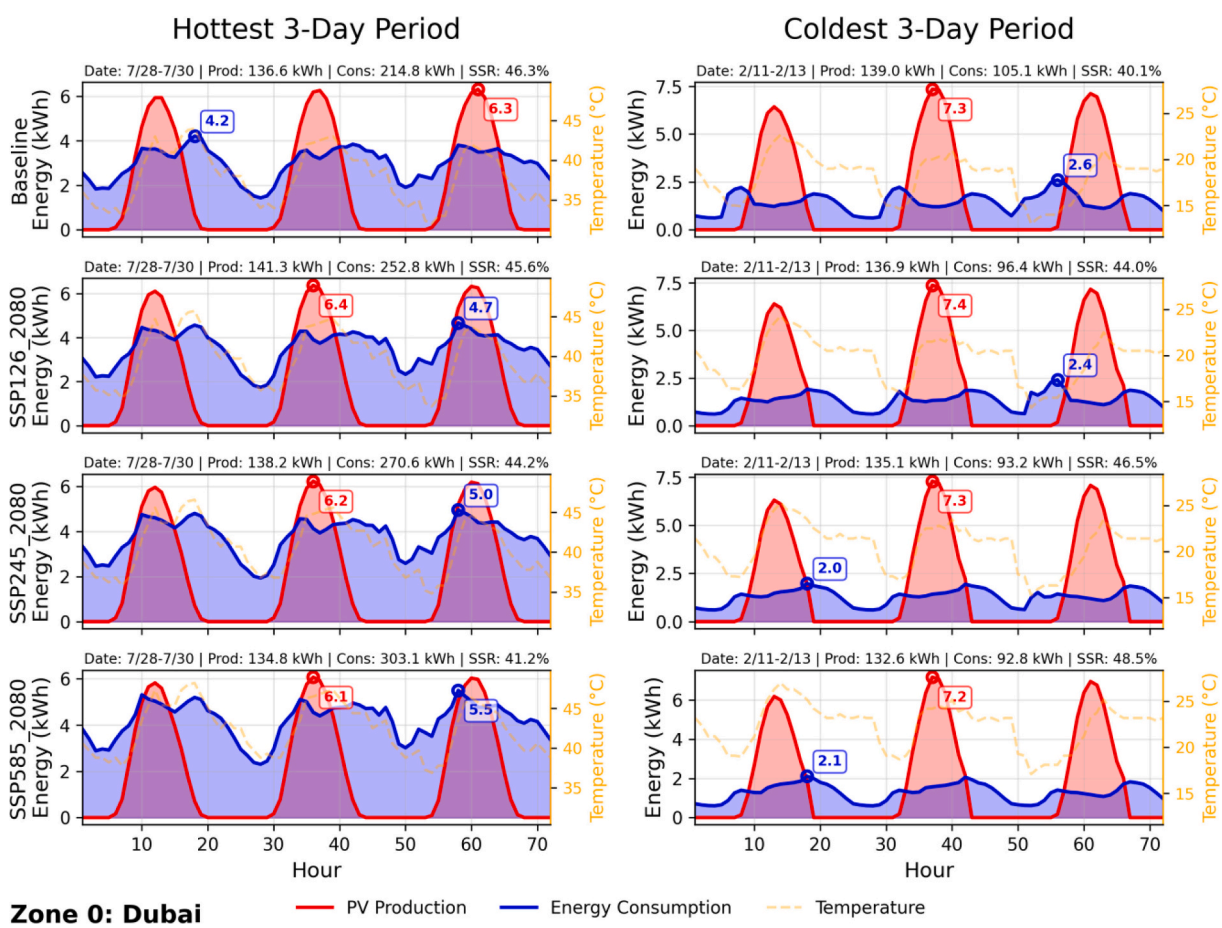


**Fig. 9.** Hourly PV generation and building demand during the hottest and coldest 3-day period for Dubai (a), Oslo (b) and Anchorage (c)

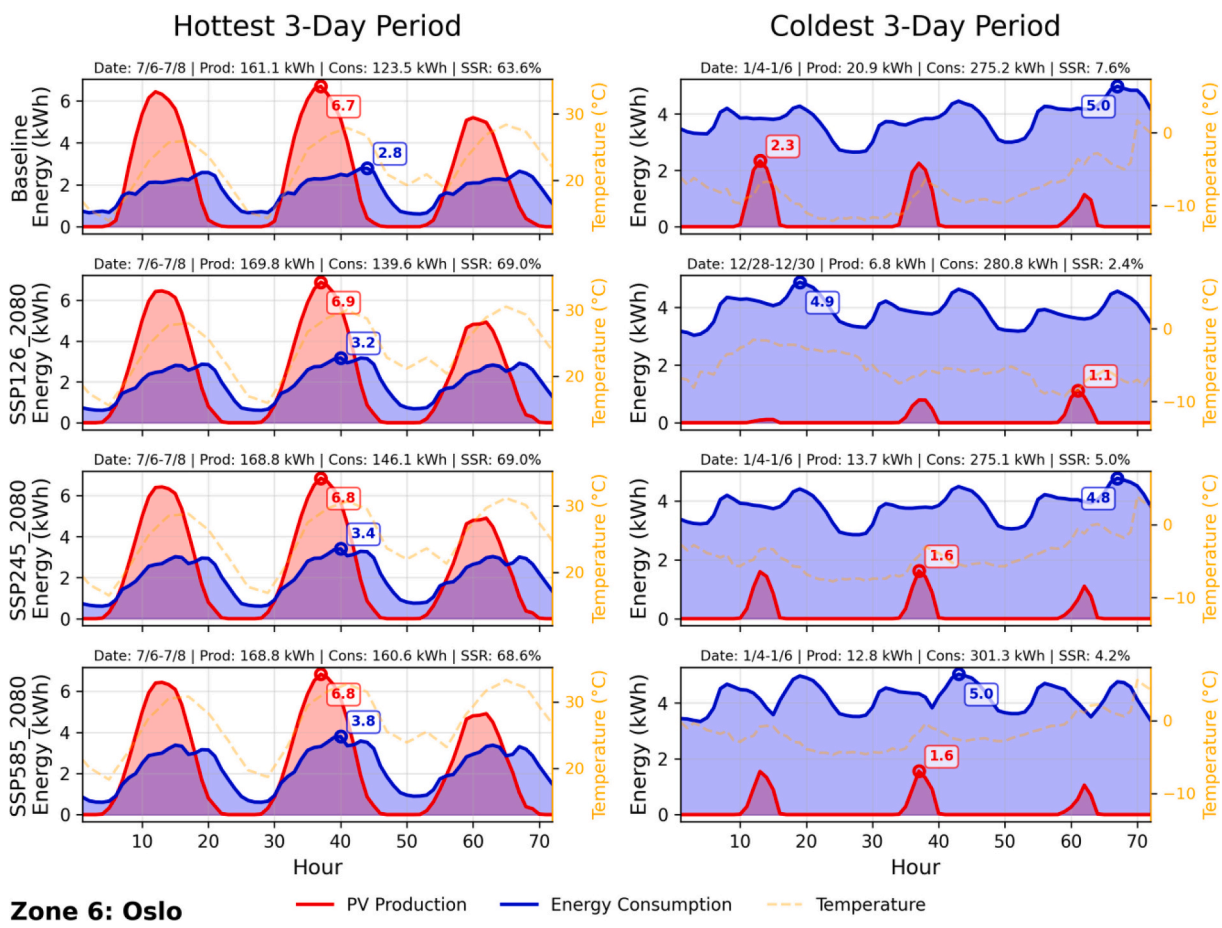


**Fig. 9.** (*continued*).

across scenarios, resulting from downscaling methodologies and global climate model uncertainties, itself illustrates the increasing unpredictability of future climate extremes.

The spatial heterogeneity of daily energy balance patterns reveals pronounced climate-dependent vulnerabilities that intensify under warming scenarios. Baseline extreme heat events create substantial energy deficits in tropical zones (Zone 0–1), with Singapore experiencing −62 kWh and Dubai −78 kWh deficits (Fig. 9a). The magnitude of these deficits under climate change underscores critical limitations in current renewable energy integration assumptions. These include Dubai's extreme heat period deficit doubling from −78 kWh to −168 kWh under SSP585_2080 while Jakarta's deficit increases by more than a factor of four, from −18 kWh to −74 kWh. Such deficits provide evidence consistent with the policy relevance of investment in grid resilience and storage infrastructure alongside distributed generation targets, though translating this evidence into specific policy instruments requires integration with economic, infrastructure, and governance considerations beyond the scope of this study.

Analysis of temporal mismatches reveals critical insights into the peak hour offset between maximum PV output (typically midday) and maximum electricity consumption. In extremely hot regions, PV production characteristically follows a bell-shaped curve with peak generation occurring between 11:00–14:00, while cooling-dominated consumption profiles exhibit extended plateau patterns with sustained high demand from 10:00–18:00. This temporal displacement creates a systematic afternoon offset, with peak or sustained cooling demand extending several hours beyond peak PV production. Under progressively severe climate scenarios, available surplus electricity during peak generation periods diminishes while deficits during low or zero PV generation periods correspondingly expand.

Singapore's hottest 3-day (Fig. S30) demonstrates a manageable misalignment between PV peaking (reaching 4.7 kWh) and consumption (reaching 3.1 kWh). However, for the SSP585_2080 scenario, these values increase to 4.8 kWh and 4.4 kWh, respectively, resulting in the SSR declining from 46.2% (baseline) to 44.4%. Technological solutions offer partial mitigation pathways. Battery and thermal energy storage integration demonstrates potential for reducing costs and life cycle impacts [71], while advanced smart control systems enable dynamic load shifting through demand response signals and optimized charging during periods of low prices or PV surplus availability. Zhan et al. [72] showed that SCR and SSR improved by 19.5% and 10.6%, respectively, using a proposed model predictive control compared to the baseline in a tropical office building. A recent machine learning study by Savino et al. [73] showed 18% energy cost reductions in Texas and 12.5% savings in California using attention-actor-critic deep reinforcement learning algorithms compared to conventional control systems. Furthermore, machine learning approaches improve SSR by 6–10.5% during constrained solar availability while reducing peak demand. These advances suggest that intelligent energy management could partially offset declining temporal alignment under climate change. They would not, however, eliminate the underlying mismatch during extreme periods if demand exceeds available on-site generation irrespective of how that generation is dispatched.

Cold climate cities (Zones 6–8) face fundamental temporal mismatches with profound system design implications. During winter extremes, limited and highly variable PV generation coincides with persistent high consumption throughout daylight hours, while peak demands often occur during morning and evening darkness. Oslo (Fig. 9b) exemplifies this challenge with peak PV generation of 6.7–6.9 kWh at 12:00 remaining relatively constant across scenarios, while

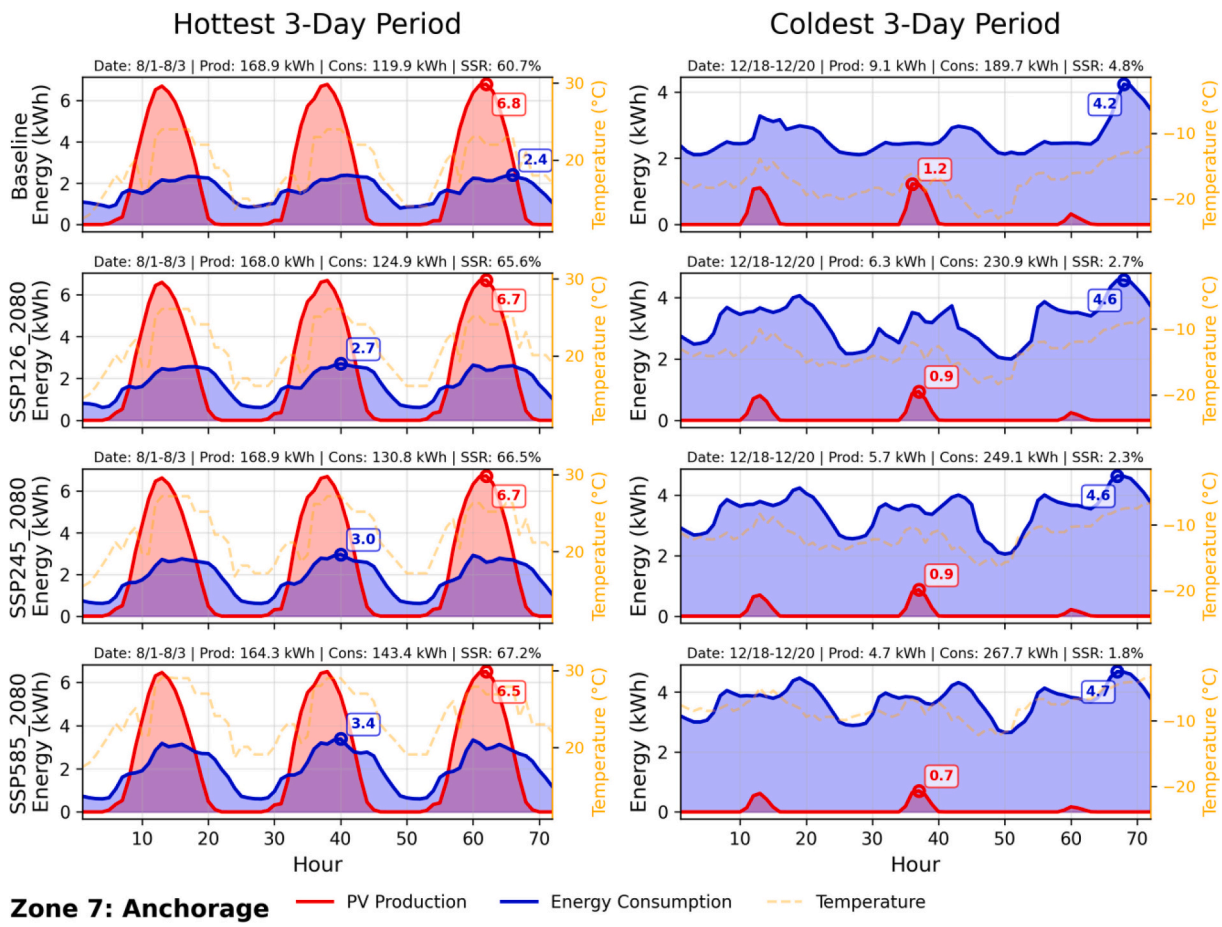


**Fig. 9.** (*continued*).

electricity demand reaches its highest levels during 13:00–19:00. This temporal variability in demand patterns under global warming adds another layer of complexity to system design.

The scale mismatch in extreme cold regions represents a major limitation to PV viability. Anchorage (Fig. 9c) peak PV production during winter extremes remains below 1.2 kWh/h, while consumption consistently exceeds 4 kWh throughout daylight hours. Complete absence of winter generation (0 kWh) in Fairbanks (Fig. S52) starkly illustrates the physical impossibility of solar self-sufficiency in polar regions. Specifically, analysis of zero-generation days (cumulative daily PV output <0.1 kWh) reveals the frequency and persistence of this constraint. Fairbanks (Zone 8) experiences 37–42 zero-generation days annually across all climate scenarios (baseline: 37 days; SSP scenarios: 40–42 days), representing approximately 10–12% of the year. Sisimiut exhibits 52–57 zero-generation days annually (baseline: 57 days; SSP scenarios: 52 days), while Yellowknife experiences 0 days. These days cluster during the December–January polar night period, with the longest continuous zero-generation period extending 50 consecutive days in Sisimiut baseline. Climate warming provides negligible improvement in zero-generation frequency, as astronomical constraints (solar elevation below horizon) rather than temperature or atmospheric conditions determine generation capacity. The cumulative energy deficit during zero-generation periods is substantial. Fairbanks' December–January zero-generation period requires 2297 kWh of grid imports under baseline conditions for such a single-family house, increasing to 2578–3043 kWh under future scenarios (SSP245_2080: 2698 kWh; SSP585_2080: 3043 kWh). Although climate change reduces annual heating EUI, the extended polar night period amplifies winter deficits. In Sisimiut, the shortened polar night duration under warming scenarios reduces the deficit from 5588 kWh (baseline) to 4594–5113 kWh (SSP126_2080: 5050 kWh; SSP585_2080: 4594 kWh).

While energy storage can provide short-term load balancing [27], extended winter generation deficits often exceeding weeks imply that battery-based seasonal storage would face substantial technical and scale challenges in these locations, noting that a full techno-economic assessment of storage feasibility is beyond this study's scope. This persistent temporal misalignment highlights a fundamental challenge for PV systems that climate change fails to resolve and may actually exacerbate in regions experiencing intensified extreme events. The resilience implications extend beyond individual building energy balance to grid-scale stability and community energy security in polar regions. These physical findings suggest that complementary technologies (wind generation, geothermal systems, or district heating networks) warrant investigation as necessary rather than optional complements to PV in subarctic climates; they also indicate that grid resilience planning should account for extended zero-generation periods, though the precise policy or infrastructure response requires analysis beyond the simulation presented here.

Regarding energy balance at extreme temperature events (Fig. S55), cold regions (Zones 6–8) exhibit remarkably heterogeneous responses during extreme heat events. While certain locations maintain positive energy balances across all scenarios (Aarhus: 15–45 kWh; Anchorage: 21–49 kWh), others undergo fundamental transitions from energy surplus to deficit (Stockholm: +11 kWh to −34 kWh). This divergent pattern reveals complex interactions between: regional solar radiation trends, temperature response, and non-linear relationships governing both PV efficiency and HVAC system performance. Particularly concerning is the widespread transition to negative balances under severe warming scenarios: Brisbane shifts from +29 to −19 kWh, and Barcelona from +25 to −41 kWh. These transitions indicate that even

temperate zones may lose their capacity for energy self-sufficiency during extreme events.

Analysis of SSR patterns during extreme events (Fig. S56) reveals paradoxical patterns. During extreme heat events, SSRs demonstrate robust renewable self-sufficiency (35.5–69.0%, average 56.7%). Unexpectedly, several high-latitude locations achieve remarkably high summer SSRs: Fairbanks (60.2–65.2%), Oslo (63.6–69.0%), and Edmonton (62.2–64.2%). This counterintuitive finding reflects extended daylight hours combined with moderate cooling demands. Polar zone analysis reveals striking internal variability: Fairbanks exhibits the highest SSR but decreasing trends, whereas Sisimiut shows the lowest values with a highly fluctuating trend.

However, these apparent summer improvements mask a fundamental seasonal asymmetry that undermines system viability. Winter extremes remain extremely poor across high-latitude regions (Oslo: 2.4–7.6%, Anchorage: 1.8–4.8%, Fairbanks: 0.0%), revealing extreme seasonal vulnerability that persists despite global warming. This profound seasonal disparity constitutes a fundamental challenge for PV system design in high-latitude regions. Most importantly, Fairbanks maintains an absolute 0% SSR during the coldest day, attributable to limited solar availability or complete polar night conditions. This necessitates a critical reassessment of renewable energy policies regarding PV deployment proportions in these regions. The persistent seasonal energy gap is consistent with the hypothesis that climate-adaptive renewable energy strategies in these regions would benefit from hybrid renewable technologies.

Fig. S56 also reveals a consistent pattern where coldest 3-day SSRs remain substantially lower than corresponding hottest 3-day values. For most cities in Zones 2–6, coldest 3-day SSRs persistently remain below 30%, indicating fundamental system limitations rather than marginal performance constraints, and these values remain insufficient to achieve meaningful energy self-sufficiency. More concerning is the degradation of SSR during extreme cold events in some representative cold climate cities despite overall improvements in annual energy balance, for example Zurich experiences a SSR decline from 26.8% to 20.8%. Paradoxically, energy consumption during extreme cold events does not consistently follow the decreasing pattern observed in annual heating demand trends but instead demonstrates intensification in several cities. Harbin (Fig. S51) exemplifies this counterintuitive pattern with 3-day consumption increasing from 158 (baseline) to 184 (SSP126_2080), 209 (SSP245_2080) and 251 kWh (SSP585_2080). Similarly, Anchorage exhibits escalation from 190 to 231, 249 and 268 kWh across the same scenarios (Fig. S49).

This phenomenon suggests that extreme weather events create acute supply-demand mismatches that differ fundamentally from average conditions. The disconnect between improved annual energy balance and deteriorating extreme event performance has critical implications for grid stability and building resilience during the most challenging operational conditions. These findings do not directly model grid stability, curtailment behavior, or outage probability; such analysis would require explicit grid-level simulation beyond the scope of this study. However, the scale of these deficits is consistent with findings from Xu et al. [36], who demonstrated super-linear growth in renewable system failure probability during extreme events. Hurricanes and severe storms can devastate solar generation through both immediate physical damage and prolonged cloud cover, creating compound vulnerabilities when building energy demands peak. Hong et al. [22] emphasized thermal resilience challenges when supply shortfalls coincide with peak demand. This poses severe challenges to public health systems and increases heat-related mortality risks [74], particularly among vulnerable populations [75]. The scale of projected energy deficits identified here provides a physically grounded basis for hypothesis generation: whether these deficits translate to grid stress or outage risk depends on storage capacity, demand response availability, and grid interconnection factors not modeled in this analysis.

Compounding these challenges is the well-documented phenomenon of temperature-induced PV and cooling efficiency degradation [23,76]. Silicon-based PV modules typically experience efficiency losses of up to 0.5% per degree Celsius above standard test conditions [23,77]. Furthermore, cooling system COP decreases as ambient temperature increases, further compounding the supply-demand mismatch during extreme heat events [16,54]. This degradation becomes critical in extreme hot regions where temperatures may reach 50.5 °C under SSP585_2080 in Dubai, particularly during intensified extreme heatwaves. The PV heat island effect further exacerbates efficiency penalties by elevating surrounding air and surface temperatures [78,79], emphasizing the need for innovative cooling strategies for PV systems. Recent experimental studies in tropical regions by Chen et al. [80] in Hong Kong and by Feng et al. [81] in Singapore demonstrate that PV-integrated green roof systems effectively lower PV surface temperatures through evapotranspiration while simultaneously reducing building heat conduction, thereby offering dual benefits of improved PV efficiency and decreased cooling demands.

### 3.4. Sensitivity and uncertainty analysis

To assess the robustness of our climate zone-specific findings to key modeling assumptions, we conducted sensitivity analyses examining critical parameters: building envelope thermal performance (Fig. S57–65), PV system capacity (Fig. S66–74) and GCM uncertainties (Table S5). Representative cities were selected in each climate zone to capture diverse thermal profiles.

#### 3.4.1. Building envelope

Building envelope retrofits represent a significant capital investment for improving energy efficiency. This analysis examines whether upgrading from older building standards to contemporary high-performance envelopes meaningfully improves PV-building temporal matching, or whether climate forcing effects dominate retrofit benefits. We compared four building vintages corresponding to successive ASHRAE Standard 90.1 / IECC code cycles: Pre_1980, 2004, 2010 and 2019, with progressively stringent envelope requirements (Table S3).

Baseline retrofits from Pre_1980 to 2019 standard for Singapore (Fig. 10), reduce total EUI from 110.2 to 96.1 kWh/m$^2$ (14.1 kWh/m$^2$, 12.9% improvement), driven entirely by cooling demand reduction from 37.8 to 27.0 kWh/m$^2$ (28.6% reduction). Grid electricity purchases decrease from 8218 to 7432 kWh annually (9.6% decrease), while surplus exports increase from 3963 to 5411 kWh (36.5% increase). Under SSP585_2080, retrofit benefits intensify: EUI declines from 156.3 to 132.4 kWh/m$^2$ (23.9 kWh/m$^2$, 15.3% improvement), with cooling falling from 79.3 to 60.5 kWh/m$^2$ (23.8% reduction). Purchased electricity decreases from 13,022 to 10,794 kWh (17.1% decrease), while exports increase from 1574 to 3119 kWh (98.2% increase). These dramatic improvements demonstrate that envelope retrofits become increasingly valuable under climate change as cooling demands escalate.

Despite substantial energy savings, SSR declines modestly from 52.7% (Pre_1980) to 50.9% (2019) at baseline and shows minimal change under SSP585_2080 (47.1% to 48.2%). This apparent contradiction, substantial energy savings yet declining or minimal SSR improvement, reflects temporal load distribution rather than retrofit ineffectiveness. Envelope improvements reduce cooling loads most effectively during nighttime and early morning hours when outdoor temperatures are lowest and solar heat gain is minimal. Peak cooling demands during midday solar-generation hours remain relatively high due to persistent internal gains, plus continued solar heat gain through windows. Consequently, retrofits reduce total consumption (reducing grid dependence) but do not proportionally shift remaining loads into solar-coincident hours (limiting SSR improvement). This pattern indicates that hot climate retrofits deliver clear energy and economic benefits through absolute consumption reduction, though they should be complemented by shading strategies, thermal storage or load

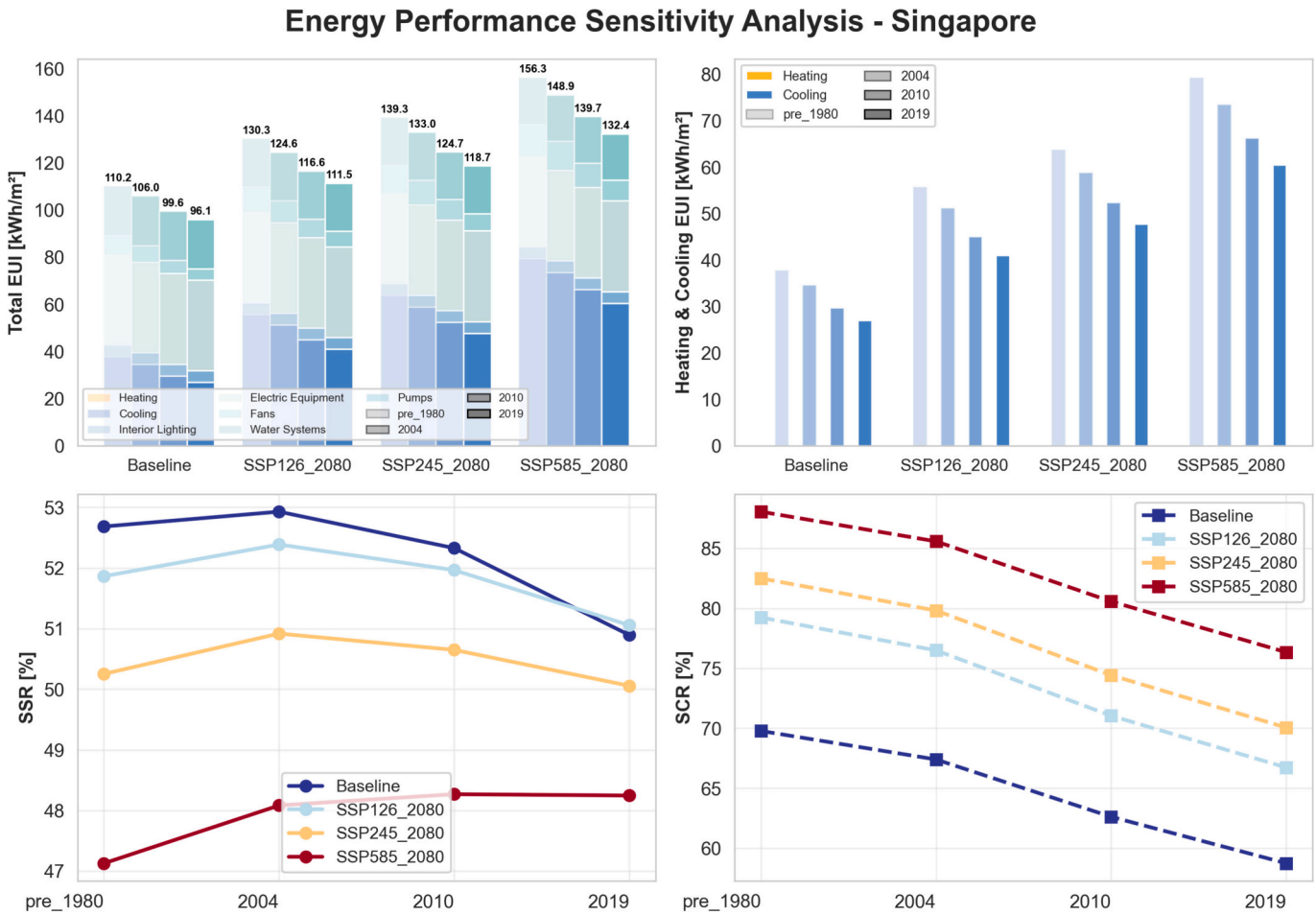


**Fig. 10.** Different building envelope thermal performance for Zone 0: Singapore.

scheduling to maximize renewable energy utilization during peak generation periods.

Transitional climate zones demonstrate remarkable stability and even improvements in PV-building performance. Cape Town (Fig. S60) demonstrates optimal retrofit performance with dual thermal benefits. Baseline retrofits reduce EUI from 93.7 (Pre_1980) to 87.3 (2019) kWh/m$^2$ (6.3 kWh/m$^2$, 6.8% improvement), with both heating declining from 16.8 to 14.5 kWh/m$^2$ (13.7% reduction) and cooling decreasing from 4.6 to 1.9 kWh/m$^2$ (58.6% decrease). Purchased electricity drops from 8834 to 8325 kWh (5.8% reduction), while exports increase from 10,786 to 11,276 kWh (4.5% increase). Under SSP585_2080, climate adaptation benefits emerge prominently. Retrofits reduce EUI from 87.7 to 79.9 kWh/m$^2$ (8.8% decrease), with heating declining from 5.1 to 4.5 kWh/m$^2$ while improved envelopes suppress emerging cooling demands from 11.3 to 5.9 kWh/m$^2$ (47.8% decrease). Purchased electricity decreases from 6986 to 6742 kWh (3.5% decrease), while exports increase from 9509 to 10,486 kWh (10.3% increase).

SSR shows modest declines from 40.1% (Pre_1980) to 39.5% (2019) at baseline, and 49.4% to 46.5% under SSP585_2080. While these modest SSR reductions might initially appear concerning, they must be interpreted within the context of substantial absolute energy savings and improved grid interactions documented above. The SSR decline occurs because envelope improvements reduce cooling loads during PV-generation hours, thereby reducing the amount of PV electricity that can be consumed on site. However, from a practical building performance perspective, the 6.8–8.8% total energy reduction, 4–11% increase in export capacity, and 3–6% decrease in purchased electricity represent clear operational and economic benefits that far outweigh the modest SSR metric change.

Cold climate retrofits deliver large absolute savings while improving renewable integration metrics. Baseline retrofits reduce EUI for Stockholm (Fig. S63) from 172.4 to 150.6 kWh/m$^2$ (12.6% improvement), driven by heating demand reduction from 86.4 to 67.4 kWh/m$^2$ (19.0 kWh/m$^2$, 22.0% reduction). The large absolute savings reflect the dominant role of heating in cold climate energy profiles and the effectiveness of envelope improvements in reducing continuous thermal losses. Purchased electricity decreases from 21,714 to 18,499 kWh (14.8% reduction), while exports increase from 4435 to 4645 kWh (4.8% increase). Critically, SSR improves from 20.0% (Pre_1980) to 22.1% (2019). Under SSP585_2080, climate warming reduces heating demands (57.3 kWh/m$^2$ for pre-1980, to 45.0 kWh/m$^2$ for 2019). Purchased electricity decreases from 16,998 (Pre_1980) to 14,861 kWh (2019) (12.6% reduction), with SSR improving from 24.7% to 26.5%, demonstrating persistent retrofit effectiveness despite natural climate benefits. This improvement occurs because envelope retrofits reduce continuous background heating loads throughout all hours including daytime periods when PV generation is available. Unlike hot climates where cooling concentrates during peak solar hours (limiting retrofit benefits for PV matching), cold climate heating occurs continuously, meaning envelope improvements reduce demands during both solar and non-solar hours. This creates the favorable outcome of absolute energy reduction accompanied by improved temporal matching with available PV resources. However, absolute SSR values remain below 36% across all selected cities in Zone 4–8, confirming that envelope improvements alone cannot overcome the fundamental astronomical constraints limiting winter PV generation in high-latitude regions.

The relationship between energy savings and self-sufficiency metrics reveals critical distinctions. Cold climates demonstrate aligned benefits

where envelope improvements simultaneously reduce consumption and improve SSR. Hot climates show divergent patterns where substantial consumption reductions from pre-1980 to 2019 across all scenarios (12.9–15.3% in Singapore) are accompanied by declining or minimal SSR improvement, indicating that energy efficiency and renewable self-sufficiency represent partially independent optimization objectives. This divergence occurs due to temporal load distribution: in hot climates, envelope improvements reduce cooling demand partly outside peak PV-generation hours, while in cold climates they reduce more continuous heating loads across both solar and non-solar periods.

These findings establish that envelope improvements deliver value through multiple benefits: (1) substantial energy savings (cost), (2) decreased grid dependence, (3) increased distributed generation, and (4) climate adaptation resilience. The comprehensive performance improvements, particularly substantial energy savings in cold climates and cooling-load suppression in transitional climates under warming, establish envelope retrofits as critical climate adaptation strategies that deliver energy, economic and grid-interaction benefits independent of specific self-sufficiency metric changes.

### 3.4.2. PV sizing

PV system capacity scaling analysis examines whether observed climate-driven SSR deterioration patterns represent capacity limitations or fundamental temporal mismatches (details in SM Fig. S66–74). We analyzed capacity variations from 50% to 150% of the baseline system (10.08 kW).

Singapore (Fig. S66) exemplifies the futility of capacity scaling in addressing temporal supply-demand mismatches characteristic of tropical cooling-dominated buildings. Increasing PV capacity from 50% (6556 kWh annual production) to 150% (19,669 kWh) yields SSR improvement from 40.4% to 54.0%. The marginal effectiveness collapses dramatically: the first 50% capacity increase (50% to 100%) produces 10.5% SSR improvement, while the final increment (100% to 150%) yields only 3.1%, a 70% degradation in marginal returns within a single capacity doubling. The annual result: 150% baseline capacity exports 11,500 kWh (58.5% of production) while still purchasing 6964 kWh (7432 kWh baseline), demonstrating that invested capacity serves only to create midday grid export burdens rather than improving building energy independence. The purchased electricity trajectory exposes diminishing returns quantitatively: 50% to 100% capacity reduces purchases 1591 kWh (9023 to 7432 kWh, 17.6% reduction), 100% to 150% reduces purchases only 468 kWh (7432 to 6964 kWh, 6.3% reduction). Each successive 50% capacity investment yields progressively smaller absolute benefits while linearly increasing capital costs, operations and maintenance expenses, and roof space requirements.

Capacity expansion beyond 125% in tropical climates reaches a physical diminishing-returns threshold in terms of energy performance gains. This surplus during midday time cannot be utilized on-site without storage, cannot be exported during high-solar-penetration scenarios without grid curtailment, and provides zero benefit during critical evening deficit periods. The climate change dimension compounds this physical limitation: capacity investments intended to improve resilience are increasingly consumed by demand escalation under warming scenarios, delivering progressively smaller absolute SSR gains, a pattern that has implications for system planning even before economic considerations are applied.

Cape Town (Fig. 11) demonstrates superficially superior capacity scaling (increasing PV capacity from 50% to 150% yields 7.2% SSR improvement baseline, 7.5% under SSP585_2080). The 100% to 150% capacity increment produces only a 2.2% SSR gain under both scenarios, indicating that the diminishing returns are as severe as those in Singapore despite fundamentally different load profiles. Although

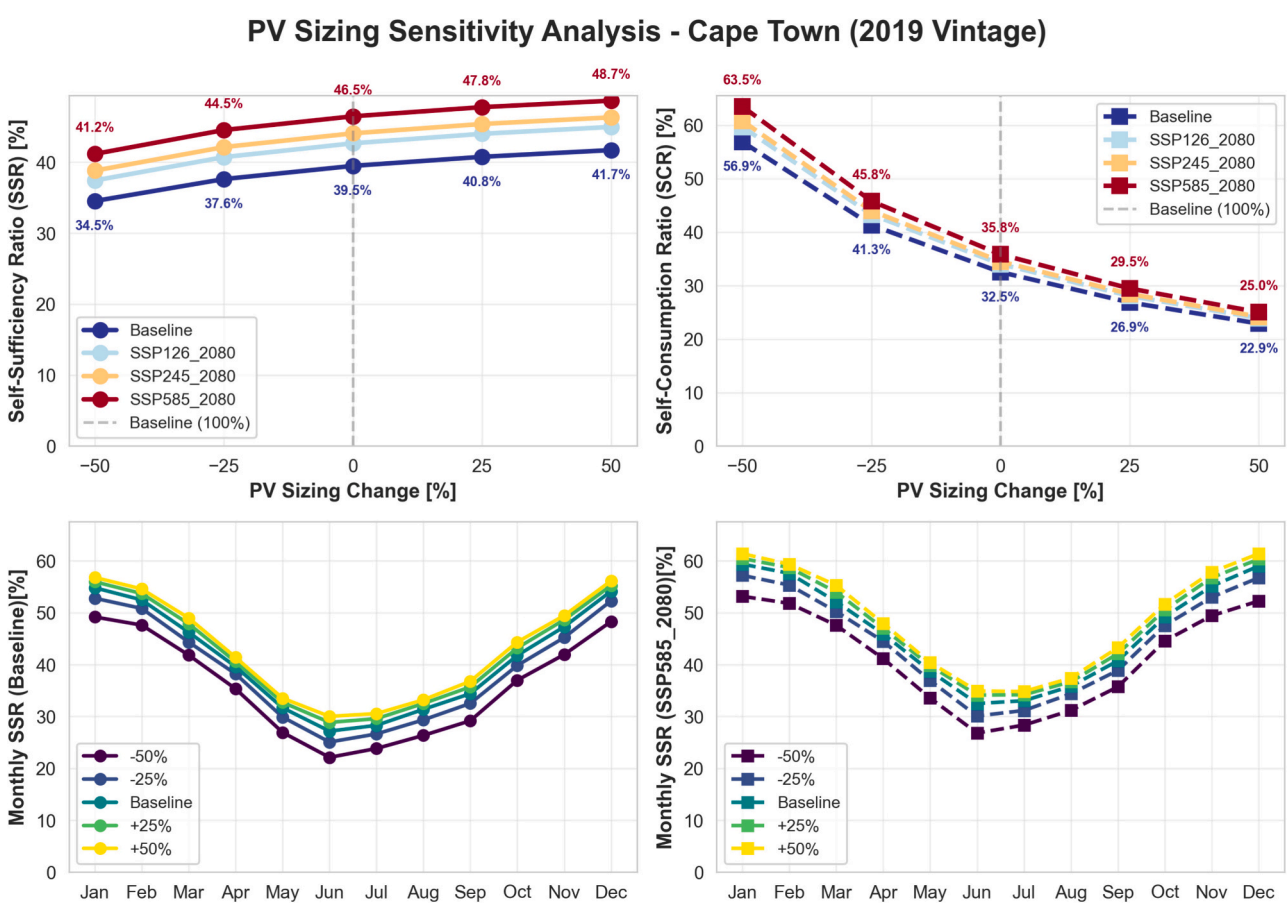


**Fig. 11.** PV sizing sensitivity analysis of Cape Town.

capacity increases from 50% to 150%, June SSR improves only from approximately 22.1% to 30.0% because generation timing fundamentally misaligns with heating demand timing. Summer months (November–March) show cooling-dominated loads with better temporal alignment (>40%), but even 150% capacity cannot fully serve demands due to late-afternoon deficits. Cape Town undergoes thermal profile transformation. Under SSP585_2080, June SSR improves from 26.8% to 34.9% from 50% to 150% capacity. Grid dependency patterns expose the optimization ceiling. Purchased electricity decreases from 9007 kWh (50% capacity, baseline) to 8019 kWh (150% capacity), merely 11.0% reduction for 200% capacity investment. Under warming, the reduction improves to 12.8% (7411 to 6465 kWh), yet the physical benefit remains limited: tripling capacity reduces grid dependence by only one-eighth, with a large amount of generation redirected to exports (from 2984 to 18,379 kWh) rather than improving SSR.

Cape Town represents the "best case" transitional climate scenario yet still demonstrates severe capacity scaling limitations. The 100–125% capacity range represents an apparent optimization window where SSR (39.5% to 40.8% baseline) improves modestly while exports remain somewhat controlled. Insufficient capacity for winter heating mismatches versus excessive capacity for summer cooling periods. Capacity shifts toward 125–150% to compensate for demand increases would also create grid integration burdens, notably annual exports of ~15–19 MWh. These burdens would require curtailment or on-site storage, which the incremental 2–3% SSR improvement does not physically warrant.

Cold climates exhibit dramatically flatter SSR-capacity relationships, revealing fundamental constraints on winter renewable viability regardless of system sizing. Stockholm (Fig. S72) demonstrates baseline SSR improvement from 16.4% (50% capacity) to 25.4% (150% capacity). Under SSP585_2080, the gradient remains similarly constrained: 20.0% to 29.8%. Even at 150% capacity, which would require either higher-efficiency modules or additional mounting beyond the current 70 $m^2$ roof constraint, winter SSR remains below 15%. This capacity-invariant winter limitation confirms that astronomical constraints, not system undersizing, determine cold climate PV viability. December–January SSR remains below 5% in Fairbanks (Fig. S74) due to polar night conditions, while summer months (Jun-July) achieve 43.7–71.9% SSR for different sizing systems.

Stockholm 150% capacity requires 17,713 kWh annual grid purchases at baseline, 74.6% of total consumption. Under warming with 150% capacity, purchases decrease to 14,202 kWh but still represent 70.2% of consumption. By contrast, surplus generation is substantial: at 150% capacity, exports amount to 8800 kWh (baseline) and 8422 kWh (SSP585_2080), representing 59.4% and 58.3% of total PV production, respectively. These statistics expose a devastating paradox: Stockholm's PV systems export 60% of generation while requiring 70–75% grid imports to cover annual consumption, indicating that capacity and demand are temporally decoupled to a degree that system sizing cannot bridge.

The marginal SSR improvement from 125% to 150% capacity (approximately 1.5%) translates to roughly 300–350 kWh additional on-site consumption annually, equivalent to 1.5% of total building consumption. The astronomical constraints that create near-zero winter generation cannot be overcome by capacity scaling; only seasonal thermal storage (may be challenging at residential scale), alternative renewable sources (wind maintains winter productivity), or district heating connections (leveraging geographic/temporal load diversity) may address winter deficits meaningfully.

A further parameter not tested in the current sensitivity analysis is PV panel tilt angle. The current simulation uses a south-facing fixed-tilt array at the roof pitch angle (22°) for all cities. For Stockholm (latitude 59.3°N), Jacobson and Jadhav [82] report a PVWatts-derived optimal tilt of 41°, which is 19° steeper than the modeled configuration. Babatunde et al. [83] demonstrate that PV plant (25° south-facing tilt) yields approximately 17.3% higher than a low-tilt array (6° tilt) based on a case study in North Cyprus. Capacity scaling increases total annual generation without altering its seasonal distribution and therefore cannot replicate this tilt-driven mechanism. PV systems with higher tilt angles tend to achieve improved performance during winter months, while systems with lower tilt angles exhibit enhanced energy output during the summer season due to seasonal variations in solar altitude. Dedicated tilt optimization analysis across high-latitude cities is identified as a priority for future simulation work.

PV capacity scaling encounters climate-specific but universally severe constraints rooted in temporal generation-demand mismatches that system sizing cannot resolve. The sensitivity analysis reveals a critical finding: observed SSR degradation is fundamentally climate-driven rather than capacity-limited. All climate zones exhibit severe diminishing returns beyond 100–125% capacity. This climate-capacity paradox exposes the futility of addressing climate-induced energy imbalances through PV capacity alone. The evidence conclusively establishes that thermal and electrical energy storage, demand-side management, hybrid renewable portfolios (PV + wind + geothermal) and grid infrastructure investment are not optional complements to PV capacity expansion but rather essential prerequisites for achieving energy independence objectives. Capacity scaling alone, regardless of magnitude, cannot overcome climate-driven temporal mismatches that characterize building energy consumption patterns across all climate zones.

### 3.4.3. Climate model uncertainty

Individual EnergyPlus simulations were conducted for all 23 CMIP6 GCMs for three representative cities spanning hot (Singapore, ASHRAE Zone 0), transitional (Cape Town, ASHRAE Zone 3), and cold (Stockholm, ASHRAE Zone 6) climates across all three SSP scenarios at the 2080 horizon. Results are presented in Fig. 12 and Supplementary Table S5. Each boxplot summarizes the distribution of simulated outcomes across the 23 GCMs; the horizontal dashed line denotes the baseline value for each city. The per-GCM bounds reported in this section are available only for the three representative cities and only at the 2080 horizon. They are not available for the remaining cities or for any derived output, including the extreme-event energy deficit and zero-generation metrics, all of which are based on the single ensemble-mean morphed weather file. The three-city spreads should therefore be read as an indicative characterization of inter-model uncertainty rather than as bounds that can be generalized to the full 27-city set or to the extreme-event results.

The baseline SSR for Singapore is 50.9%. Under SSP126, the 23-GCM mean SSR remains effectively stable at 51.0% (range: 50.5–51.7%), as marginal PV yield gains under mild warming are offset by rising cooling demand. Under SSP245 and SSP585, SSR declines progressively to means of 49.9% (range: 49.3–50.7%) and 48.1% (range: 46.9–49.5%), respectively. Critically, the SSP585 mean SSR falls below the minimum SSR produced by any individual GCM under SSP126, confirming that the progressive SSR deterioration in hot climates is a robust cross-model finding rather than a model-dependent artifact. EUI increases substantially across all GCMs without exception, from a baseline of 96.1 kWh/$m^2$ to means of 111.3, 118.5 and 132.1 kWh/$m^2$ under SSP126, SSP245 and SSP585, respectively. The inter-model spread in EUI widens with emissions intensity (105.1–116.8 kWh/$m^2$ under SSP126 versus 120.4–144.8 kWh/$m^2$ under SSP585), consistent with the known amplification of CMIP6 model uncertainty under high forcing scenarios. SCR rises markedly under all scenarios, from a baseline of 58.7% to a SSP585 mean of 75.9% (range: 71.4–80.2%), reflecting the increasing fraction of PV output consumed on-site as cooling loads intensify.

The baseline SSR for Cape Town is 39.5%, the highest of the three cities, reflecting the favorable solar resource characteristic of its Mediterranean climate (baseline PV production: 16709 kWh/year) combined with a relatively low building energy demand (baseline EUI: 87.3 kWh/$m^2$). Under all SSP scenarios, SSR improves monotonically across all 23 GCMs, driven by reductions in a mildly heating-dominated building load that progressively outweigh modest increases in cooling demand. Under

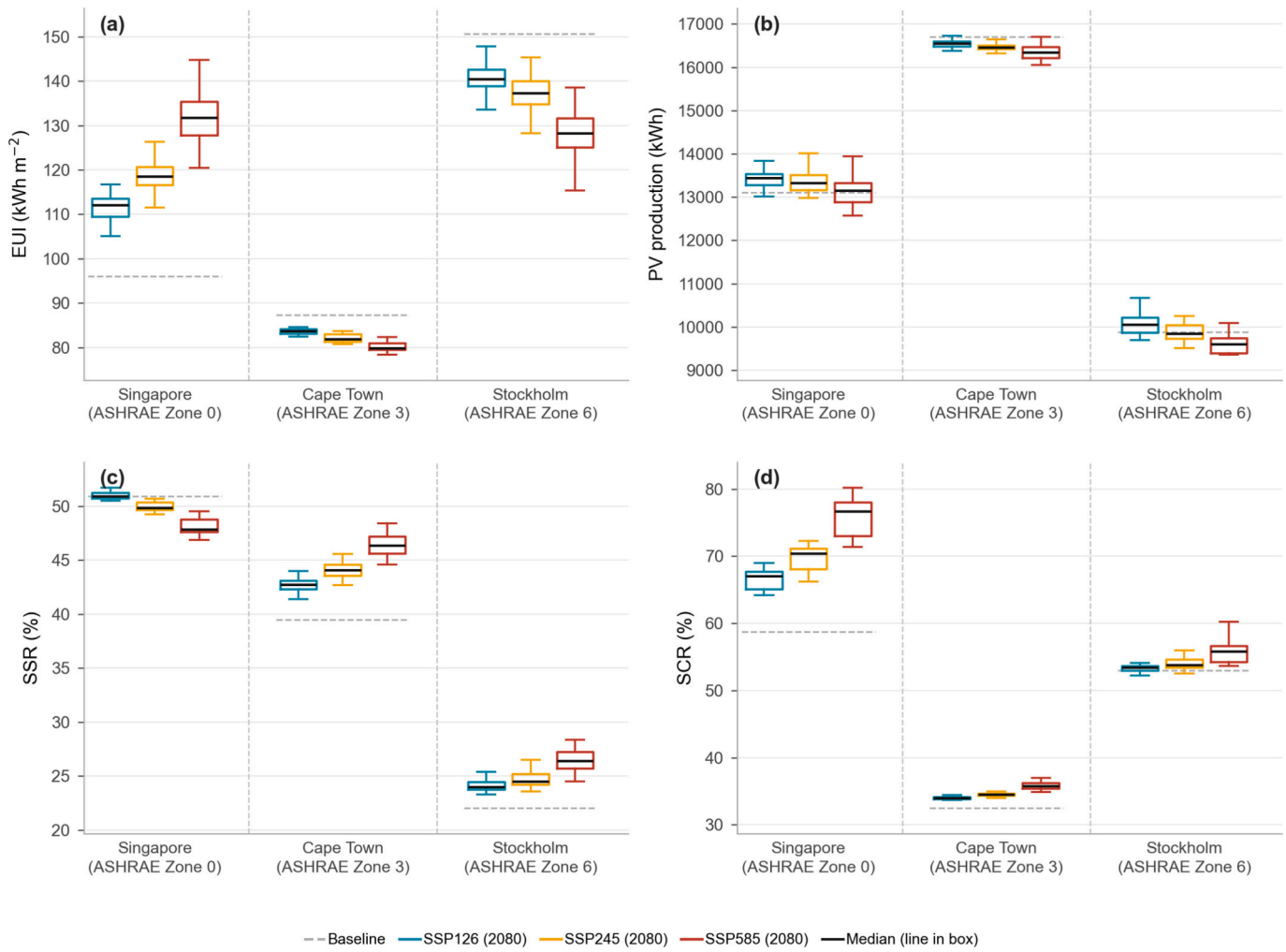


**Fig. 12.** Inter-model uncertainty in (a) EUI (kWh/m$^2$), (b) annual PV production (kWh), (c) SSR (%), and (d) SCR (%) across 23 CMIP6 GCMs for three representative cities (Singapore, Cape Town and Stockholm) for 2080.

SSP126, SSP245, and SSP585, the mean SSR reaches 42.7% (range: 41.4–44.0%), 44.1% (range: 42.7–45.6%), and 46.4% (range: 44.6–48.4%), representing improvements of approximately 3.2, 4.6 and 7.0 percentage points above the baseline, respectively. EUI declines consistently across all 23 GCMs, from a baseline of 87.3 kWh/m$^2$ to a SSP585_2080 mean of 80.2 kWh/m$^2$ (range: 78.4–82.3 kWh/m$^2$). The inter-model spread in SSR for Cape Town is moderate and consistent across scenarios (2.6 pp. under SSP126, 2.9 pp. under SSP245, 3.8 pp. under SSP585), reflecting GCM divergence in projected precipitation and cloud cover changes over the southern African Mediterranean region. Importantly, no GCM contradicts the direction of SSR improvement or EUI reduction for Cape Town under any scenario, confirming the robustness of the warm-temperate zone findings.

The baseline SSR for Stockholm is 22.1%, the lowest of the three cities, reflecting severe solar resource constraints at high latitudes combined with a large heating-dominated building load. Under all SSP scenarios, SSR improves consistently across all 23 GCMs, driven by progressive reductions in heating energy demand as the climate warms. Under SSP126, SSP245 and SSP585, the mean SSR reaches 24.3% (range: 23.3–26.0%), 24.8% (range: 23.6–27.3%), and 26.6% (range: 24.5–29.8%), representing improvements of approximately 2.2, 2.7 and 4.5 percentage points above the baseline, respectively. EUI declines across all GCMs, from a baseline of 150.6 kWh/m$^2$ to a SSP585 mean of 128.5 kWh/m$^2$ (range: 115.4–138.6 kWh/m$^2$), primarily driven by heating EUI. The inter-model spread in EUI for Stockholm is notably wide under SSP585, reflecting GCM divergence in projected Arctic amplification and the sensitivity of heating loads to winter temperature projections. Importantly, despite this spread, the direction of change is consistent across the entire 23 GCMs: every model projects SSR improvement and EUI reduction for Stockholm under every scenario, supporting the conclusion that cold-climate heating load reductions under warming constitute a robust finding.

The three cities reveal contrasting climate-zone responses that are each internally consistent across 23 GCMs. Singapore exhibits narrow SSR spread (no more than 2.7 percentage points) but wide EUI spread under high forcing, reflecting GCM disagreement in tropical warming intensity. Cape Town shows moderate SSR spread (up to 3.8 percentage points under SSP585) alongside the largest absolute SSR improvement of the three cities (7.0 percentage points under SSP585), underpinned by strong solar resource availability and progressive heating load elimination. Stockholm shows the widest absolute EUI spread (up to 23.2 kWh/m$^2$ under SSP585), driven by divergence in high-latitude winter warming projections. The direction of change in SSR and EUI is consistent across all three cities and all three SSP scenarios.

### 3.5. Policy and practice implications

The complex spatial and temporal disparities documented in this analysis demand that policymakers transition from universal renewable energy targets to climate-specific strategies. These approaches must explicitly address temporal dynamics between supply and demand, particularly as climate change fundamentally alters building energy.

Addressing fundamental energy mismatches requires prioritizing demand-side interventions tailored to climate-specific challenges, with both tropical and cold regions requiring distinct but complementary approaches to optimize renewable energy integration potential. These interventions provide immediate benefits while simultaneously reducing carbon emissions that drive warming, creating compounding positive effects for both energy performance and climate mitigation. For tropical regions (Zones 0–1), mandatory envelope performance standards represent the highest-return intervention, with our sensitivity analysis demonstrating cooling demand reductions of 23.8–33.4% when upgrading from pre-1980 construction to contemporary ASHRAE 2019 standards. Singapore specifically achieves 18.9 kWh/m$^2$ annual cooling savings under SSP585_2080 through envelope retrofits, translating to substantial grid electricity import reductions of 17.1% (13,022 to 10,794 kWh). These improvements should target high-performance thermal envelopes with solar heat gain control, such as advanced glazing systems with appropriate SHGC, smart shading, cool/green envelopes and enhanced airtightness to minimize cooling loads during peak solar hours. This demand-side approach addresses the fundamental mismatch problem at its source. Second, strategic PV capacity optimization policies should mandate system sizing matched to daytime cooling loads rather than arbitrary capacity targets, as our analysis reveals that oversized systems face declining marginal returns. Third, short-duration thermal storage systems and strategies like pre-cooling could be incentivized to address the critical temporal offset between peak PV generation and peak cooling demand [84,85]. For regions experiencing large diurnal temperature variations, policies and building codes could incentivize thermal storage utilizing phase change materials or other innovative technologies to optimize temporal energy matching.

Transitional climate zones (Zones 2–3) require distinctly different priorities centered on adaptive flexibility rather than unidirectional optimization. Cape Town exemplifies regions undergoing fundamental thermal profile transformations, shifting from heating-dominated conditions (baseline heating/cooling ratio: 7.6) to balanced situations (0.8 under SSP585_2080). For these regions, policy frameworks could prioritize hybrid HVAC system requirements that mandate reversible heat pump systems capable of efficiently serving both heating and cooling loads as seasonal patterns shift, addressing profile transformation more cost-effectively than separate equipment. Envelope optimization should balance dual-season performance requirements by combining appropriate insulation levels with solar heat gain control strategies.

For cities in Zones 6–8, comprehensive demand-side interventions remain critically important despite climate warming benefits. While heating demands decrease under warming scenarios, heating continues to dominate energy consumption with minimal improvements in winter SSR. Policy frameworks should prioritize building envelope retrofit programs, supported by analysis showing heating reductions of 18.3–26.0% (Zones 4–8) through upgrades from pre-1980 construction standards to ASHRAE 2019 specifications. These retrofits deliver the highest absolute energy savings (9.1–14.7% reduction in total consumption) and improve annual SSR despite persistent winter limitations. Priority should be given to envelope measures targeting air infiltration reduction, improved window and insulation performance, and the mitigation of thermal bridges to achieve substantial heating load reductions that complement renewable energy systems.

Critically, cold climate policies should explicitly mandate hybrid renewable energy systems as a second-tier priority, acknowledging that PV alone cannot serve as a standalone renewable solution. Our zero-generation day analysis quantifies this fundamental limitation, with the longest continuous period extending 50 consecutive days during polar night. These extended generation deficits suggest that seasonal battery storage alone would face substantial physical barriers given the scale of supply gaps documented here, a finding consistent with the broader literature on high-latitude renewable integration [27]. Complementary technologies, including wind generation for winter baseload, heat pumps, or district heating networks with thermal storage [71], warrant investigation as necessary complements to PV. Despite winter limitations, summer performance remains strong (SSR 50–70% during extreme heat events), suggesting that policies could optimize PV systems for maximum summer generation while accepting winter grid dependence rather than oversizing systems that produce excessive summer exports with minimal winter benefit.

Finally, comprehensive grid infrastructure modernization and performance assessment frameworks should evolve to accommodate the heterogeneous impacts of climate change on building and renewable energy systems. Grid modernization policies should account for bidirectional energy flows (imports and exports) with climate-responsive variability. Importantly, building performance metrics and renewable energy targets should incorporate temporal matching indicators, rather than relying solely on annual energy balances. Aggregate annual metrics obscure the challenges associated with extreme-day performance, which is expected to influence grid stability and building resilience at scales beyond the single building modeled here.

Current climate zone classification systems do not incorporate solar radiation as a classification parameter, despite its critical importance for renewable energy system performance. This study's reliance on ASHRAE thermal zones means that cities grouped together may experience divergent PV performance trajectories. Future research should advocate for and utilize climate classification frameworks that integrate both thermal characteristics and solar resource metrics. As solar technologies become increasingly critical for achieving net-zero energy buildings and decarbonization targets, a comprehensive climate classification framework that simultaneously captures thermal loads (heating/cooling) and renewable generation potential (solar resources) would provide more robust guidance for building design, energy policy development and technology deployment strategies.

These contrasting vulnerability patterns across climate zones challenge simplistic adaptation strategies and highlight the need for regionally differentiated approaches to PV implementation under global warming. The intuitive assumption that increased solar radiation under climate change would universally benefit PV generation is contradicted by our analysis, which reveals complex, location-specific responses that demand carefully tailored policy and technical solutions.

## 4. Limitations and outlook

This study acknowledges several limitations that warrant future consideration. First, methodological constraints related to the building archetype approach limit the generalizability of findings. The use of a single residential archetype, while enabling systematic cross-climate comparison, does not capture the performance variations inherent in different building types, occupancy patterns and envelope specifications. Future research should extend this analysis to include multi-family apartments, townhouses and commercial buildings to establish the broader applicability of our climate-zone-specific findings. The standardized design parameters, uniform internal gains and fixed occupancy schedules represent reasonable contemporary practice but may not reflect regional construction variations, cultural differences in space usage or future efficiency improvements.

Second, the sensitivity analysis is limited in its representation of both supply-side and demand-side temporal dynamics. PV capacity scaling does not account for tilt angle variation, which increases annual generation without altering the seasonal distribution of output, and therefore cannot capture potential winter generation improvements achievable through latitude-optimized tilt configurations in high-latitude cities. Dedicated PV tilt optimization is therefore identified as a priority for future work. In addition, key operational parameters governing temporal load distribution, including occupancy schedules, internal heat gain profiles, infiltration and ventilation rates, HVAC setpoints, and domestic hot water usage, remain fixed at standardized values across all simulations. The implications of these assumptions for temporal supply–demand alignment, particularly under cooling-

dominated conditions in hot climates and heating-dominated conditions in cold climates, remain insufficiently explored and warrant targeted investigation. In addition, all city-by-scenario results are derived from a single ensemble-mean morphed weather file per city, scenario and period. Per-GCM uncertainty bounds were generated only for three representative cities. Full inter-model uncertainty bands are therefore not available for the remaining cities or for derived extreme-event deficit and zero-generation metrics, and the reported three-city spreads should not be extrapolated to the full city set.

Third, the instantaneous energy balance approach assumes perfect grid availability without considering technical or economic constraints. These simplifications enable consistent cross-climate comparison but do not capture the full complexity of real-world grid interactions, including electricity tariff structures [86], net-metering policy restrictions [87], export curtailment during periods of grid over-generation [88], or grid capacity constraints during peak demand periods. The analysis should therefore be interpreted as documenting temporal mismatch patterns and their evolution under climate change, rather than as direct predictions of grid infrastructure stress or reliability outcomes. Battery storage analysis, which would require co-simulation of storage dispatch strategies, degradation modeling and techno-economic optimization, represents an essential but distinct research question beyond the scope of this study's focus.

This study focuses on physical energy performance dynamics rather than economic optimization and environmental impact assessment. As a result, economic metrics such as levelized cost of energy, net present value, or internal rate of return fall outside our current scope. In addition, operational emissions quantification requires specification of location-specific and temporally dynamic grid emission factors, future decarbonization pathways and detailed modeling of building-grid interactions including net metering and marginal emissions displacement. These factors introduce substantial uncertainty and warrant dedicated investigation.

Future research should address these limitations by expanding the analytical scope from static assumptions toward active adaptation strategies. Building on the temporal mismatch patterns identified in this study, load-shifting strategies, such as rescheduling domestic hot water heating, appliance operation, and pre-conditioning to align with peak PV generation, represent a promising demand-side intervention to improve temporal matching. This is particularly relevant in hot climates where midday PV availability coincides with cooling demand, and in cold climates where heating loads typically precede winter solar availability. Systematic evaluation of load flexibility potential across climate zones is therefore identified as an important avenue for future work.

Beyond individual buildings, future studies should employ integrated co-simulation frameworks incorporating battery storage, demand response, vehicle-to-grid systems, PV cooling technologies (including green and cool roof integration), and intelligent energy management systems. Most importantly, because the present single-building analysis cannot represent grid-outage behavior or microgrid feasibility, greater attention should be paid to the interaction between urban-scale building energy demand and microgrid systems, which would require dedicated system-level co-simulation to capture the effects of urban morphology, microclimate interactions, mutual shading, population growth, cooling adoption trends, and rebound effects that increasingly shape real-world energy system performance.

## 5. Conclusion

This study investigates building rooftop PV performance across diverse ASHRAE climate zones under global warming, revealing fundamental spatiotemporal heterogeneities. Through examination of annual, monthly and daily performance metrics on a representative single-storey house across 27 cities, this study reveals that building energy performance and PV generation exhibit disproportionate responses to climate change, creating fundamental temporal misalignments. Sensitivity analysis examining building envelope performance variations and PV system capacity changes demonstrated that climate-driven vulnerability patterns remain consistent across parameter ranges. The key findings include:

At the annual resolution, our findings demonstrate pronounced divergence in energy performance trajectories between climate zones. Extreme hot regions (Zone 0) face compound vulnerabilities, with total energy consumption increasing by 19.0–24.6% (SSP245_2080) and 33.6–38.5% (SSP585_2080), while SSRs deteriorate from baseline values of 48.2–50.9% to 46.5–49.0% under SSP585_2080. This deterioration occurs despite increased SCRs (rising to 62.1–76.3%), indicating that PV generation becomes increasingly inadequate to meet escalating cooling demands. Conversely, cool and cold climate regions (Zones 5–6) experience energy consumption reductions of 8.4–12.8% (SSP245_2080) and 11.3–19.5% (SSP585_2080) with corresponding improvements in annual energy balance, though SSR remains constrained at 23.0–34.0% (SSP245_2080) and 24.0–35.6% (SSP585_2080) due to persistent temporal mismatches. Transitional zones (Zones 2–3) emerge as potentially optimal locations for PV deployment, maintaining positive energy balances (Cape Town) while demonstrating resilience under a changing climate.

Regarding monthly analysis, hot climate regions exhibit systematic degradation in grid exchange profiles. Cold regions in Zones 6–8 demonstrate persistent seasonal asymmetry, with winter SSR typically remaining below 15% despite temperature increases of 4–7 °C, confirming that astronomical constraints rather than temperature limitations determine high-latitude renewable performance. Particularly significant are threshold transitions in temperate zones, where months traditionally dominated by heating loads shift to cooling-dominated profiles, fundamentally altering building rooftop PV performance dynamics and necessitating reconceptualization of HVAC system design strategies.

Daily extreme events analysis exposes critical vulnerabilities determining system resilience and grid stability. Hottest 3-day periods exhibit high SSRs (35.5%–69.0%, average 56.7%), while coldest 3-day periods show substantially lower values (0–51.4%, average 23.5%) for all scenarios, with some locations experiencing zero generation during polar nights. Specifically, Fairbanks experiences 37–42 zero-generation days annually (10–12% of the year), while Sisimiut shows 52–57 days, with the longest continuous zero-generation period extending 50 consecutive days. During extreme heat events, energy deficits in hot regions nearly double in Dubai (−78 to −168 kWh) and increase approximately fourfold in Jakarta (−18 to −74 kWh) under SSP585_2080, while SSRs decline precisely when cooling demands peak. These deficit values are derived from the ensemble-mean weather file and are not accompanied by inter-model uncertainty bounds. These extreme disparities indicate potential stress on grid infrastructure and occupant health during periods when energy systems are most vulnerable, although grid-level outcomes depend on storage, demand response and network factors not modeled in this single-building analysis.

These multiscale findings necessitate a fundamental reconceptualization of building energy policies. Universal renewable energy targets must yield to climate-specific frameworks that explicitly address temporal dynamics. For tropical regions, policies should prioritize demand-side interventions through stringent building codes and renovations minimizing cooling loads during solar peaks, coupled with short-duration thermal storage to bridge temporal mismatches. Our sensitivity analysis demonstrates that envelope improvements following higher standards can partially offset climate-driven SSR deterioration, though they cannot fully eliminate compound vulnerabilities in extreme hot climates. Cold regions should emphasize comprehensive envelope renovations and hybrid energy strategies. These building-scale results suggest that future grid integration will need to account not only for bidirectional flows but for shifts in their magnitude and timing under a changing climate. Most importantly, performance metrics must evolve beyond annual energy balances to incorporate temporal matching

indicators and extreme event resilience, as these factors ultimately determine real-world system viability. These insights provide essential guidance for future grid design and planning, particularly as zero-emissions policies increasingly rely on substantial solar PV integration within electrical infrastructure.

As climate change accelerates and renewable energy becomes increasingly critical for decarbonization, understanding these complex spatiotemporal dynamics becomes essential for designing resilient, locally tailored, climate-responsive building energy systems. The findings indicate the importance of moving away from one-size-fits-all approaches and the assumption that PV alone is sufficient, in favor of tailored strategies that integrate efficient building energy management and comprehensive renovation strategies for better utilization of solar resources under global warming. All results reported here describe the energy balance of a single residential building archetype under a simplified instantaneous grid-exchange assumption. They do not constitute validated grid-outage, curtailment, or microgrid feasibility conclusions, which would require explicit system-level modeling of storage dispatch, demand response, and grid interconnection beyond the boundary of this study.

## CRediT authorship contribution statement

**Zhuocheng Duan:** Writing – review & editing, Writing – original draft, Visualization, Validation, Software, Resources, Methodology, Investigation, Formal analysis, Data curation, Conceptualization. **Shady Attia:** Writing – review & editing, Supervision. **Hossein Omrany:** Writing – review & editing, Supervision, Funding acquisition. **Ruidong Chang:** Writing – review & editing. **Jian Zuo:** Writing – review & editing, Supervision.

## Declaration of competing interest

The authors declare that they have no known competing financial interests or personal relationships that could have appeared to influence the work reported in this paper.

## Acknowledgments

This research was supported by the Australian Government Research Training Program Scholarship and the Ian Wilson Liberal Foundation Research Supplementary Scholarship. This study resulted from a collaborative research visit to Prof. Shady Attia at the University of Liège, Belgium, funded by the Hans-Jürgen and Marianne Ohff Research Grant.

## Appendix A. Supplementary data

Supplementary data to this article can be found online at https://doi.org/10.1016/j.apenergy.2026.128210.

## Data availability

No data was used for the research described in the article.

## References

[1] Schleussner C-F, Rogelj J, Schaeffer M, Lissner T, Licker R, Fischer EM, et al. Science and policy characteristics of the Paris agreement temperature goal. Nat Clim Change 2016;6:827–35. https://doi.org/10.1038/nclimate3096.
[2] United Nations. THE 17 GOALS | sustainable development. https://sdgs.un.org/goals. [Accessed 27 March 2025].
[3] UNEP. Global status report for buildings and construction: beyond foundations - mainstreaming sustainable solutions to cut emissions from the buildings sector. United Nations Environment Programme; 2023. p. 2024. https://doi.org/10.59117/20.500.11822/45095.
[4] IEA. Buildings - energy system, IEA. https://www.iea.org/energy-system/buildings; 2024 (accessed January 3, 2025).
[5] Duan Z, De Wilde P, Attia S, Zuo J. Challenges in predicting the impact of climate change on thermal building performance through simulation: a systematic review. Appl Energy 2025;382:125331. https://doi.org/10.1016/j.apenergy.2025.125331.
[6] Yan D, Wu Y, Malik J, Hong T. Ten questions on future and extreme weather data for building simulation and analysis in a changing climate. Build Environ 2025; 269:112461. https://doi.org/10.1016/j.buildenv.2024.112461.
[7] Zeng Z, Kim J-H (Jeannie), Tan H, Hu Y, Cameron-Rastogi P, Villa D, et al. A review of future weather data for assessing climate change impacts on buildings and energy systems. Renew Sustain Energy Rev 2025;212:115213. https://doi.org/10.1016/j.rser.2024.115213.
[8] Duan Z, de Wilde P, Attia S, Zuo J. Prospect of energy conservation measures (ECMs) in buildings subject to climate change: a systematic review. Energ Buildings 2024;322:114739. https://doi.org/10.1016/j.enbuild.2024.114739.
[9] Shen P, Li Y, Gao X, Zheng Y, Huang P, Lu A, et al. Recent progress in building energy retrofit analysis under changing future climate: a review. Appl Energy 2025;383:125441. https://doi.org/10.1016/j.apenergy.2025.125441.
[10] Belcher S, Hacker J, Powell D. Constructing design weather data for future climates. Building Services Engineering Research and Technology 2005;26:49–61. https://doi.org/10.1191/0143624405bt112oa.
[11] Jentsch MF, James PAB, Bourikas L, Bahaj AS. Transforming existing weather data for worldwide locations to enable energy and building performance simulation under future climates. Renew Energy 2013;55:514–24. https://doi.org/10.1016/j.renene.2012.12.049.
[12] Rodrigues E, Fernandes MS, Carvalho D. Future weather generator for building performance research: an open-source morphing tool and an application. Build Environ 2023;233:110104. https://doi.org/10.1016/j.buildenv.2023.110104.
[13] Shen P. Building and urban simulation under future climate: a novel statistical downscaling method for future hourly weather data generation. Building Simulation 2025. https://doi.org/10.1007/s12273-025-1277-z.
[14] de Wilde P, Coley D. The implications of a changing climate for buildings. Build Environ 2012;55:1–7. https://doi.org/10.1016/j.buildenv.2012.03.014.
[15] Jalali Z, Shamseldin AY, Ghaffarianhoseini A. Impact assessment of climate change on energy performance and thermal load of residential buildings in New Zealand. Build Environ 2023;243:110627. https://doi.org/10.1016/j.buildenv.2023.110627.
[16] Wang H, Chen Q. Impact of climate change heating and cooling energy use in buildings in the United States. Energ Buildings 2014;82:428–36. https://doi.org/10.1016/j.enbuild.2014.07.034.
[17] Zou Y, Xiang K, Zhan Q, Li Z. A simulation-based method to predict the life cycle energy performance of residential buildings in different climate zones of China. Build Environ 2021;193:107663. https://doi.org/10.1016/j.buildenv.2021.107663.
[18] Rahif R, Norouziasas A, Elnagar E, Doutreloup S, Pourkiaei SM, Amaripadath D, et al. Impact of climate change on nearly zero-energy dwelling in temperate climate: time-integrated discomfort, HVAC energy performance, and GHG emissions. Build Environ 2022;223:109397. https://doi.org/10.1016/j.buildenv.2022.109397.
[19] Akkose G, Akgul C Meral, Dino IG. Educational building retrofit under climate change and urban heat island effect. J Build Eng 2021;40:102294. https://doi.org/10.1016/j.jobe.2021.102294.
[20] International Renewable Energy Agency (IRENA), solar energy. https://www.irena.org/Energy-Transition/Technology/Solar-energy; 2025 [accessed March 27, 2025].
[21] Kuhn TE, Erban C, Heinrich M, Eisenlohr J, Ensslen F, Neuhaus DH. Review of technological design options for building integrated photovoltaics (BIPV). Energ Buildings 2021;231:110381. https://doi.org/10.1016/j.enbuild.2020.110381.
[22] Hong T, Malik J, Krelling A, O'Brien W, Sun K, Lamberts R, et al. Ten questions concerning thermal resilience of buildings and occupants for climate adaptation. Build Environ 2023:110806. https://doi.org/10.1016/j.buildenv.2023.110806.
[23] Aspetakis G, Wang Q. Critical review of air-based PVT technology and its integration to building energy systems. Energy Built Environ 2025;6:121–35. https://doi.org/10.1016/j.enbenv.2023.10.001.
[24] De Masi RF, Festa V, Gigante A, Mastellone M, Ruggiero S, Vanoli GP. Effect of climate changes on renewable production in the Mediterranean climate: case study of the energy retrofit for a detached house. Sustainability 2021;13:8793. https://doi.org/10.3390/su13168793.
[25] Liu L, He G, Wu M, Liu G, Zhang H, Chen Y, et al. Climate change impacts on planned supply–demand match in global wind and solar energy systems. Nat Energy 2023;8:870–80. https://doi.org/10.1038/s41560-023-01304-w.
[26] Tamer T, Gürsel Dino I, Akgül C Meral. Data-driven, long-term prediction of building performance under climate change: building energy demand and BIPV energy generation analysis across Turkey. Renew Sustain Energy Rev 2022;162: 112396. https://doi.org/10.1016/j.rser.2022.112396.
[27] D'Agostino D, Parker D, Epifani I, Crawley D, Lawrie L. How will future climate impact the design and performance of nearly zero energy buildings (NZEBs)? Energy 2022;240:122479. https://doi.org/10.1016/j.energy.2021.122479.
[28] Ahmadian E, Bingham C, Elnokaly A, Sodagar B, Verhaert I. Impact of climate change and technological innovation on the energy performance and built form of future cities. Energies 2022;15:8592. https://doi.org/10.3390/en15228592.
[29] Guo J, Chen Z, Meng J, Zheng H, Fan Y, Ji L, et al. Picturing China's photovoltaic energy future: insights from CMIP6 climate projections. Renew Sustain Energy Rev 2024;189:114026. https://doi.org/10.1016/j.rser.2023.114026.
[30] Jerez S, Tobin I, Vautard R, Montávez JP, López-Romero JM, Thais F, et al. The impact of climate change on photovoltaic power generation in Europe. Nat Commun 2015;6:10014. https://doi.org/10.1038/ncomms10014.

[31] Luthander R, Widén J, Nilsson D, Palm J. Photovoltaic self-consumption in buildings: a review. Appl Energy 2015;142:80–94. https://doi.org/10.1016/j.apenergy.2014.12.028.
[32] Ciocia A, Amato A, Di Leo P, Fichera S, Malgaroli G, Spertino F, et al. Self-consumption and self-sufficiency in photovoltaic systems: effect of grid limitation and storage installation. Energies 2021;14:1591. https://doi.org/10.3390/en14061591.
[33] Bertsch V, Geldermann J, Lühn T. What drives the profitability of household PV investments, self-consumption and self-sufficiency? Appl Energy 2017;204:1–15. https://doi.org/10.1016/j.apenergy.2017.06.055.
[34] Gudmunds D, Nyholm E, Taljegard M, Odenberger M. Self-consumption and self-sufficiency for household solar producers when introducing an electric vehicle. Renew Energy 2020;148:1200–15. https://doi.org/10.1016/j.renene.2019.10.030.
[35] Nyholm E, Goop J, Odenberger M, Johnsson F. Solar photovoltaic-battery systems in Swedish households – self-consumption and self-sufficiency. Appl Energy 2016;183:148–59. https://doi.org/10.1016/j.apenergy.2016.08.172.
[36] Xu L, Lin N, Poor HV, Xi D, Perera ATD. Quantifying cascading power outages during climate extremes considering renewable energy integration. Nat Commun 2025;16:2582. https://doi.org/10.1038/s41467-025-57565-4.
[37] Bass B, New J. How will United States commercial building energy use be impacted by IPCC climate scenarios? Energy 2023;263:125945. https://doi.org/10.1016/j.energy.2022.125945.
[38] International energy conservation code (IECC), ASHRAE climatic design conditions SI help. https://ashrae-meteo.info/v2.0/help_IECC.php; 2021. [Accessed March 28, 2025].
[39] ASHRAE, ANSI/ASHRAE standard 169–2020 - climatic data for building design standards, 2021.
[40] Ciancio V, Salata F, Falasca S, Curci G, Golasi I, de Wilde P. Energy demands of buildings in the framework of climate change: an investigation across Europe. Sustain Cities Soc 2020;60:102213. https://doi.org/10.1016/j.scs.2020.102213.
[41] Khawaja SA, Memon SA. Novel indicators to evaluate PCM performance under different ventilation strategies by considering the impact of climate change. J Build Eng 2023;74:106848. https://doi.org/10.1016/j.jobe.2023.106848.
[42] Rodrigues E, Parente J, Fernandes MS. Building for tomorrow: analyzing ideal thermal transmittances in the face of climate change in Brazil. Appl Energy 2024;355:122360. https://doi.org/10.1016/j.apenergy.2023.122360.
[43] Deng Z, Javanroodi K, Nik VM, Chen Y. Using urban building energy modeling to quantify the energy performance of residential buildings under climate change. Building Simulation 2023. https://doi.org/10.1007/s12273-023-1032-2.
[44] Skandalos N, Karamanis D. Decarbonizing operational emissions in urban neighborhoods with the integration of rooftop photovoltaics and green infrastructure under current and future climate conditions. Energ Buildings 2025;329:115306. https://doi.org/10.1016/j.enbuild.2025.115306.
[45] Duan Z, Omrany H, Zuo J. Impact of climate change on energy performance and energy conservation measures effectiveness in Australian office buildings. Energy 2025;319:134956. https://doi.org/10.1016/j.energy.2025.134956.
[46] Liu S, Kwok YT, Lau KK-L, Tong HW, Chan PW, Ng E. Development and application of future design weather data for evaluating the building thermal-energy performance in subtropical Hong Kong. Energ Buildings 2020;209:109696. https://doi.org/10.1016/j.enbuild.2019.109696.
[47] Rodrigues E, Fereidani NA, Fernandes MS, Gaspar AR. Climate change and ideal thermal transmittance of residential buildings in Iran. J Build Eng 2023;74:106919. https://doi.org/10.1016/j.jobe.2023.106919.
[48] Amaripadath D, Rahif R, Zuo W, Velickovic M, Voglaire C, Attia S. Climate change sensitive sizing and design for nearly zero-energy office building systems in Brussels. Energ Buildings 2023;286:112971. https://doi.org/10.1016/j.enbuild.2023.112971.
[49] Intergovernmental panel on climate change. climate change 2021 – the physical science basis: working group i contribution to the sixth assessment report of the intergovernmental panel on climate change. 1st ed. Cambridge University Press; 2023. https://doi.org/10.1017/9781009157896.
[50] Stuecker MF, Bitz CM, Armour KC, Proistosescu C, Kang SM, Xie S-P, et al. Polar amplification dominated by local forcing and feedbacks. Nat Clim Change 2018;8:1076–81. https://doi.org/10.1038/s41558-018-0339-y.
[51] ASHRAE. Standard 100–2018 – energy efficiency in existing buildings. https://www.ashrae.org/technical-resources/bookstore/standard-100. [Accessed 10 August 2025].
[52] Mohammed A, Khan A, Saeed Khan H, Santamouris M. On the cooling energy impacts of combined urban heat mitigation strategies in subtropical urban building environment. Energ Buildings 2024;309:113918. https://doi.org/10.1016/j.enbuild.2024.113918.
[53] Burnett D, Barbour E, Harrison GP. The UK solar energy resource and the impact of climate change. Renew Energy 2014;71:333–43. https://doi.org/10.1016/j.renene.2014.05.034.
[54] Baglivo C, Congedo PM, Murrone G, Lezzi D. Long-term predictive energy analysis of a high-performance building in a mediterranean climate under climate change. Energy 2022;238:121641. https://doi.org/10.1016/j.energy.2021.121641.
[55] Barea G, Victoria Mercado M, Filippín C, Monteoliva JM, Villalba A. New paradigms in bioclimatic design toward climatic change in arid environments. Energ Buildings 2022;266:112100. https://doi.org/10.1016/j.enbuild.2022.112100.
[56] Waddicor DA, Fuentes E, Sisó L, Salom J, Favre B, Jiménez C, et al. Climate change and building ageing impact on building energy performance and mitigation measures application: a case study in Turin, northern Italy. Build Environ 2016;102:13–25. https://doi.org/10.1016/j.buildenv.2016.03.003.
[57] Chen K, Zuo J, Chang R. Compendium of degradation rates of global photovoltaic (PV) technology: insights from technology, climate and geography. Solar Energy Materials and Solar Cells 2025;293:113839. https://doi.org/10.1016/j.solmat.2025.113839.
[58] Krarti M. Evaluation of energy performance for rotating residential buildings integrated with rooftop PV systems. Appl Energy 2025;383:125407. https://doi.org/10.1016/j.apenergy.2025.125407.
[59] Ren Z, Paevere P, Chen D. Feasibility of off-grid housing under current and future climates. Appl Energy 2019;241:196–211. https://doi.org/10.1016/j.apenergy.2019.03.068.
[60] United Nations, Asia-Pacific Population and Development Report 2023, 2023, https://repository.unescap.org/items/9ca2bb0c-52c1-450c-90bc-59a32a703145 (accessed May 28, 2025).
[61] Mutschler R, Rüdisüli M, Heer P, Eggimann S. Benchmarking cooling and heating energy demands considering climate change, population growth and cooling device uptake. Appl Energy 2021;288:116636. https://doi.org/10.1016/j.apenergy.2021.116636.
[62] Berardi U, Jafarpur P. Assessing the impact of climate change on building heating and cooling energy demand in Canada. Renew Sustain Energy Rev 2020;121:109681. https://doi.org/10.1016/j.rser.2019.109681.
[63] Amaripadath D, Sailor DJ, Bertini A, Barker M, Attia S. Are net zero energy buildings necessarily also net zero emission buildings? Time-integrated analysis using dynamic grid emission factors. Build Environ 2025;283:113367. https://doi.org/10.1016/j.buildenv.2025.113367.
[64] Amaripadath D, Sailor DJ, Khan A, Bertini A, Attia S. Achieving low-carbon electricity operations in net zero energy residential buildings through plug-in battery energy storage systems. J Energy Storage 2026;153:120964. https://doi.org/10.1016/j.est.2026.120964.
[65] Su X, Huang Y, Chen C, Xu Z, Tian S, Peng L. A dynamic life cycle assessment model for long-term carbon emissions prediction of buildings: a passive building as case study. Sustain Cities Soc 2023;96:104636. https://doi.org/10.1016/j.scs.2023.104636.
[66] Shibuya T, Croxford B. The effect of climate change on office building energy consumption in Japan. Energ Buildings 2016;117:149–59. https://doi.org/10.1016/j.enbuild.2016.02.023.
[67] Havas L, Ballweg J, Penna C, Race D. Power to change: analysis of household participation in a renewable energy and energy efficiency programme in Central Australia. Energy Policy 2015;87:325–33. https://doi.org/10.1016/j.enpol.2015.09.017.
[68] Kim JD, Trevena W. Measuring the rebound effect: a case study of residential photovoltaic systems in San Diego. Utilities Policy 2021;69:101163. https://doi.org/10.1016/j.jup.2020.101163.
[69] Yamazaki S, Kotani H, Nakano K, Matsushima K. Using electric vehicles to power houses or travel during blackouts triggered by natural hazards: a choice experiment in Japan. Energ Buildings 2025:115801. https://doi.org/10.1016/j.enbuild.2025.115801.
[70] Fachrizal R, Qian K, Lindberg O, Shepero M, Adam R, Widén J, et al. Urban-scale energy matching optimization with smart EV charging and V2G in a net-zero energy city powered by wind and solar energy. eTransportation 2024;20:100314. https://doi.org/10.1016/j.etran.2024.100314.
[71] Baniasadi A, Habibi D, Al-Saedi W, Masoum MAS, Das CK, Mousavi N. Optimal sizing design and operation of electrical and thermal energy storage systems in smart buildings. J Energy Storage 2020;28:101186. https://doi.org/10.1016/j.est.2019.101186.
[72] Zhan S, Dong B, Chong A. Improving energy flexibility and PV self-consumption for a tropical net zero energy office building. Energ Buildings 2023;278:112606. https://doi.org/10.1016/j.enbuild.2022.112606.
[73] Savino S, Minella T, Nagy Z, Capozzoli A. A scalable demand-side energy management control strategy for large residential districts based on an attention-driven multi-agent DRL approach. Appl Energy 2025;393:125993. https://doi.org/10.1016/j.apenergy.2025.125993.
[74] Antoniou N, Montazeri H, Blocken B, Neophytou M. On the impact of climate change on urban microclimate, thermal comfort, and human health: multiscale numerical simulations. Build Environ 2024;260:111690. https://doi.org/10.1016/j.buildenv.2024.111690.
[75] Van Hoof J, Soebarto V, Ayalon L, Marston HR, Zander KK, Dikken J, et al. Ten questions concerning older people and a sustainable built environment. Build Environ 2025;274:112742. https://doi.org/10.1016/j.buildenv.2025.112742.
[76] Dubey S, Sarvaiya JN, Seshadri B. Temperature dependent photovoltaic (PV) efficiency and its effect on PV production in the world – a review. Energy Procedia 2013;33:311–21. https://doi.org/10.1016/j.egypro.2013.05.072.
[77] Kaldellis JK, Kapsali M, Kavadias KA. Temperature and wind speed impact on the efficiency of PV installations. Experience obtained from outdoor measurements in Greece. Renew Energy 2014;66:612–24. https://doi.org/10.1016/j.renene.2013.12.041.
[78] Elhabodi TS, Yang S, Parker J, Khattak S, He B-J, Attia S. A review on BIPV-induced temperature effects on urban heat islands. Urban Clim 2023;50:101592. https://doi.org/10.1016/j.uclim.2023.101592.
[79] Chen L, Zhang S, Cheng I, Chang H, Chen F, Li M, et al. The resilience paradox of rooftop PV: building cooling penalties and heat risks. Build Environ 2025:113233. https://doi.org/10.1016/j.buildenv.2025.113233.
[80] Chen L, Lin Z, Zhou Q, Zhang S, Li M, Wang Z. Impacts of photovoltaics and integrated green roofs on urban climate: experimental insights for urban land surface modelling. Renew Sustain Energy Rev 2025;217:115709. https://doi.org/10.1016/j.rser.2025.115709.

[81] Feng X, Zeng G, Ying C, Zainudin EB, Jusuf SK, Soh CB, et al. Analysis of microclimate and electrical performance of solar green roofs through a large-scale experimental study in a tropical microgrid. Energ Buildings 2025:115957. https://doi.org/10.1016/j.enbuild.2025.115957.
[82] Jacobson MZ, Jadhav V. World estimates of PV optimal tilt angles and ratios of sunlight incident upon tilted and tracked PV panels relative to horizontal panels. Solar Energy 2018;169:55–66. https://doi.org/10.1016/j.solener.2018.04.030.
[83] Babatunde AA, Abbasoglu S, Senol M. Analysis of the impact of dust, tilt angle and orientation on performance of PV plants. Renew Sustain Energy Rev 2018;90:1017–26. https://doi.org/10.1016/j.rser.2018.03.102.
[84] Zeng Z, Zhang W, Sun K, Wei M, Hong T. Investigation of pre-cooling as a recommended measure to improve residential buildings' thermal resilience during heat waves. Build Environ 2022;210:108694. https://doi.org/10.1016/j.buildenv.2021.108694.
[85] Naderi S, Heim D, Heslop S, Chen D, MacGill I, Sproul A, et al. Reducing greenhouse emissions from Australia's housing stock through solar pre-cooling and pre-heating. Energ Buildings 2025;336:115556. https://doi.org/10.1016/j.enbuild.2025.115556.
[86] Fridgen G, Kahlen M, Ketter W, Rieger A, Thimmel M. One rate does not fit all: an empirical analysis of electricity tariffs for residential microgrids. Appl Energy 2018;210:800–14. https://doi.org/10.1016/j.apenergy.2017.08.138.
[87] Comello S, Reichelstein S. Cost competitiveness of residential solar PV: the impact of net metering restrictions. Renew Sustain Energy Rev 2017;75:46–57. https://doi.org/10.1016/j.rser.2016.10.050.
[88] O'Shaughnessy E, Cruce JR, Xu K. Too much of a good thing? Global trends in the curtailment of solar PV. Sol Energy 2020;208:1068–77. https://doi.org/10.1016/j.solener.2020.08.075.